Received: 28 Sep 2023 | Revised: 02 Nov 2023 | Accepted: 04 Nov 2023

https://doi.org/10.56946/jce.v2i2.214

Journal of Chemistry and Environment

Review

Experimental and Theoretical Aspects of MXenes-Based Energy Storage and Energy Conversion Devices

Salamat Ali[1], Awais Ahmad[2,3], Iftikhar Hussain[4], Syed Shoaib Ahmad Shah[5], Shafqat Ali[6], Asad Ali[7],*, Muhammad Sufyan Javed[2,8*]

[1]School of Materials and Energy, Lanzhou University, Lanzhou 730000, China
[2]Department of Chemistry, The University of Lahore, Lahore, 54590, Pakistan
[3]Departamento de Química Orgánica, Universidad de Córdoba, Campus Universitario de Rabanales, Edificio Marie Curie (C3), E-14014 Córdoba, Spain
[4]Department of Mechanical Engineering, City University of Hong Kong, 83 Tat Chee Avenue, Kowloon, Hong Kong
[5]Department of Chemistry, School of Natural Sciences, National University of Sciences and Technology, Islamabad 44000, Pakistan
[6]Department of Physics, Shah Abdul Latif University Khairpur, Khairpur, Sindh, 66202, Pakistan
[7]Energy Engineering, Division of Energy Science, Luleå University of Technology, 97187 Luleå, Sweden
[8]School of Physical Science and Technology, Lanzhou University, Lanzhou 730000, China
*Corresponding authors:
safisabri@gmail.com (M.S. Javed) &
bachabjr@yahoo.com (A. Ali)

Abstract

Transition metal carbides, nitrides, and carbonitrides (MXenes) have become an appealing framework for developing various energy applications. MXenes with van der Waals (vdW) interactions are facile, highly efficient, affordable, and self-assembled features that improve energy density. MXenes exhibit large surface area, high electric conductivity, and excellent electrochemical characteristics for various energy applications. This review summarizes and emphasizes the current developments in MXene with improved performance for energy storage or conversion devices, including supercapacitors (SCs), various types of rechargeable batteries (RBs), solar cells, and fuel cells. We discuss the crystal structures of MXenes properties of MXenes and briefly discuss them for different types of energy applications. Finally, the critical outlook and perspective for the MXene progress for applications in energy applications are also described.

Keywords: MXenes, supercapacitors, capacitors, rechargeable batteries, solar cells, fuel cells.

Graphical Abstract:

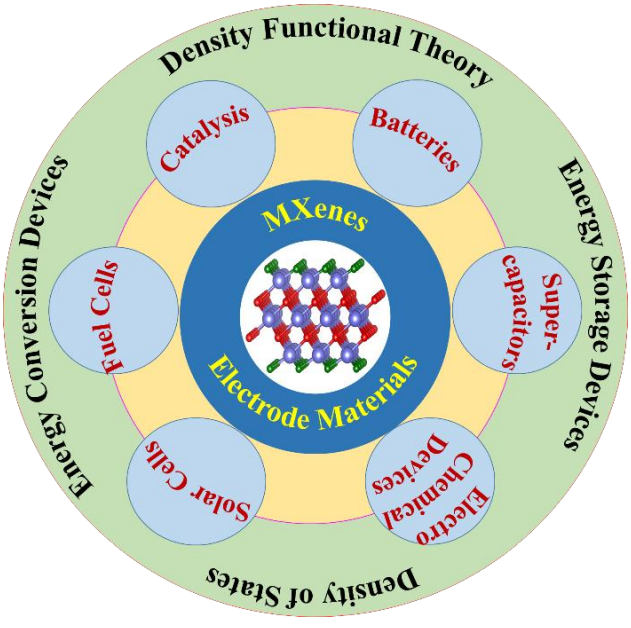

1. Introduction

Energy consumption from limited fossil fuels has increased due to global population growth and rapid industrial development [1-3]. The excessive use of these energy supplies significantly impacts the world economy and environmental protection [4, 5]. Ecologically acceptable, affordable, and viable energy production and storage technology are urgently needed to fulfill the world's rising energy demands [6, 7]. Using sustainable energy sources like solar, tidal, and wind energies are most alluring and practical strategy [8, 9]. Nevertheless, because of the abrupt climate change, the power produced from these natural resources is sporadic and unreliable [10, 11]. Following that, the most considerable difficulty is storing the electricity produced by these sources [12, 13]. To solve the issues concerning storing electrical energy, researchers have been inspired by the disadvantages above to create an efficient energy storage system with vital characteristics like high energy and power densities and outstanding cycle performance [14, 15]. This has drawn much interest to electrochemical energy storage technologies like SCs and RBs, frequently found in portable electronics like multi-media-based systems, smartphones, tablets, and health check equipment [16, 17]. The Ragone plot (Figure. 1) [18] illustrates the comparison between SCs, Cs, fuel cells, and different RBs regarding energy and power density. One of the most popular energy storage technologies, RBs, has less power than SCs, incapable of withstanding extreme temperatures, and is efficient during the charging phase of their life cycle. [19, 20]. Conventional capacitors cannot function at low temperatures, have a lower energy density, and have a longer charging-discharging time than SCs. This shows that Cs, which has an intermediate state, bridges SCs and RBs [19, 20].

Recently, producing 2D materials-based electrodes with high performance has been a significant focus because of their high specific surface area (SSA), flexibility, 2D atomic and exceptional physiochemical properties, thermal properties, electrical properties, and considerable mechanical strength [21, 22]. Researchers continuously broadened the 2D materials family after discovering the first 2D graphene material, which gained attractive attention because of their unique physical and chemical characteristics [23]. The 2D materials, including transition metal dichalcogenides (TMDs), polymer, hexagonal boron nitrides, metal oxides, MXenes, etc., show outstanding results [24]. MXenes, an emerging family of 2D materials, have drawn much interest and shown excellent performances for EES and conversion devices based on theoretical and experimental studies [25-27]. Because of their intrinsic properties, such as rich surface redox chemistry, fascinating mechanical properties, high SSA, metallic conductivity, and hydrophilicity, they are capable of fast ion transport and tunable electronic band gap, they are unique [25, 26, 28]. MXenes work exceptionally well and finding more applications, including in energy storage devices and energy conversion, etc., for improving their performances due to their characteristics [28, 29].

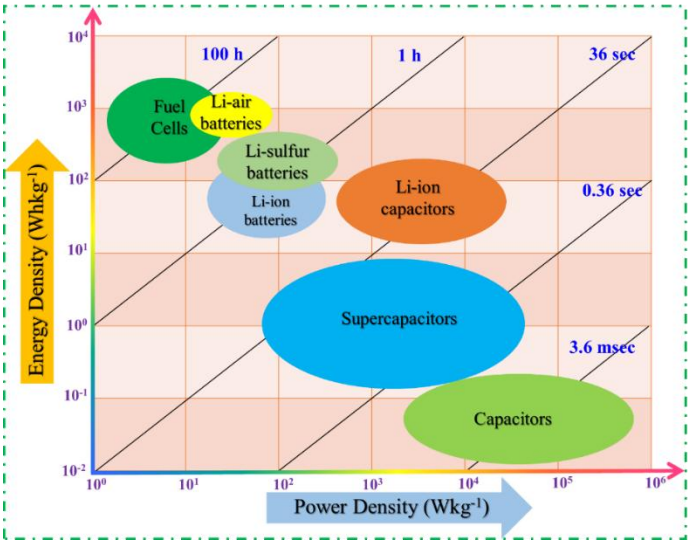

Figure 1. Ragone plot illustrating Power Density Vs. Energy Density of differ

However, several problems remain to be resolved, including low capacitance issues, weak surface functional groups, unreacted microstructure, and a tendency to aggregate or stack, which reduces the SSA; as a result, the number of active surface sites becomes less [30]. Various tactics have been used to determine these problems and enhance their performance

for energy applications, including surface modification, doping, structural control, and making MXene-based composite materials with high electrochemical performances [31, 32]. This review summarizes and focuses on current developments in MXene that have improved performance for energy storage devices and energy conversion applications such as Cs, SCs, RBs, catalysts, solar cells, and fuel cells. We briefly review the crystal structure, MXene characteristics, and their exceptional performance in energy storage devices and conversion applications. We outline the critical outlook and prospects for MXene research and development for energy storage devices and conversion applications.

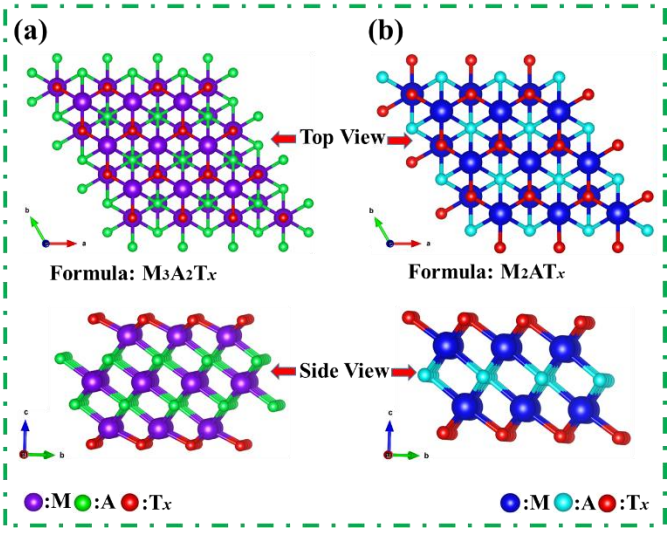

Figure 2. The crystal structures of MXene, (a) M3A2Tx, and (b) M2ATx.

2. Crystal Structures and Synthesis of MXenes

In 2011, the Gogotsi' team discovered a family of 2D metal carbides, nitrides, and carbonitrides known as MXenes ($Ti_3C_2T_x$) [33]. The MXene family has overgrown due to the MXene material's unique qualities, such as their combination of conductive features, metallic properties, and hydrophilicity [34]. MXenes' general formula is $M_{n+1}AT_x$(n = 1, 2, 3, 4) [35], where "M" stands for early transition metals (Ti, V, Nb, Mo, etc.), "A" belongs to the group III-A or IV-A, represents carbon or nitrogen and T_x stands the surface termination group $-O_2$, $-(OH)_2$, $-F_2$,. MXenes are regarded as an emerging star material due to their fascinating characteristics, including high conductive nature, increased SSA, simplicity of dispersion in solvents, and superior functionalization ability [36, 37]. MXenes utilize a pseudocapacitive behavior for a double-layer charge storage process, exhibiting rapid ion movement and redox reactions [38, 39]. MXenes are helpful for larger lithium-ion batteries (LIBs) due to their exceptional mechanical strength at the nanoscale [40, 41]. As shown in Fig. 2, MXenes come in various formulations based on their crystal structure, including M_3A_2 Fig. 2(a), M_2A, Fig. 2(b), etc.

Most reported MXenes are created by carefully choosing metallic atoms from their precursors, known as MAX, and then etching them with chemicals. In this instance, MAX phases are part of a large family of about 70 stacked carbides or nitrides [42]. The etching of the A-layers causes various surface termination groups, such as –F, –O, and –OH, to be substituted, which increases the material's hydrophilicity. Various methods are used to synthesize MXenes that comprise epitaxial growth, bottom-up approach, and top-down etching exfoliating process [43, 44]. Several procedures are available in the research, including HF etching, hydrothermal synthesis method, *in-situ* HF formation etching, alkali etching, electrochemical etching, molten salt etching, etc [45, 46]. The synthesis method of MXene from Max phases is illustrated in Table. 1.

3. Properties of MXenes

MXenes gained significant attention as an electrode material in energy storage devices and conversion systems [44, 55]. Each type of MXene has a distinct set of unique and special properties that can significantly improve the electrochemical performance of energy storage and energy conversion devices (Fig. 3). MXenes possess excellent electronic conductivity due to their metallic nature; this property allows for efficient electron transport within the material, reducing internal resistance and improving the overall performance of devices [56]. Their large SSA can accommodate more active sites for electrochemical reactions [57]. They also exhibit high ion diffusion rates because of their open, layered structure, which enables fast charge/discharge rates in devices, making them suitable for high-power applications [58].

Table 1. Synthesis methods of MXene from MAX phases.

Methods	MXene	Parent MAX phases	Etchants	Etchant condition	Surface Group	Ref
HF etching	$Ti_3C_2T_x$	Ti_3AlC_2	50 wt% HF	RT, 2 h	—OH, —O, —F	[47]
HF etching	V_2CT_x	V_2AlC	50 wt% HF	RT, 90 h	___	[48]
HF etching	Nb_2CT	Nb_2AlC	50 wt% HF	RT, 90 h	___	[48]
HF etching	$Ta_4C_3T_x$	Ta_4AlC_3	50 wt% HF	RT, 72 h	___	[42]
In-situ HF formation etching	Ti_2CT_x	Ti_2AlC	6 M LiF + 0.9 M HCl	40 °C, 15 h	—OH, —O, —F	[49]
In-situ HF formation etching	$Ti_3C_2T_x$	Ti_3AlC_2	1 M $NaHF_2$	60 °C, 24 h	—OH, —O, —F	[50]
Alkali etching	$Ti_3C_2T_x$	Ti_3AlC_2	1 M NaOH + 1 M H_2SO_4	80 °C, 100 h + 80 °C, 2 h	—OH, —O	[51]
Electrochemical etching	$Ti_3C_2T_x$	Ti_3AlC_2	1 M NH_4Cl + 0.2 M TMAOH	5 V, 5 h	—OH, —O, —Cl	[52]
Molten salt etching	Ti_2CT_x	Ti_2AlC	$ZnCl_2$	550 °C, 5 h, Ar	—O, —Cl	[53]
Other etching methods	Mo_2C	Mo_2Ga_2C	Ultraviolet light (100 W)	3–5 h	—O	[54]

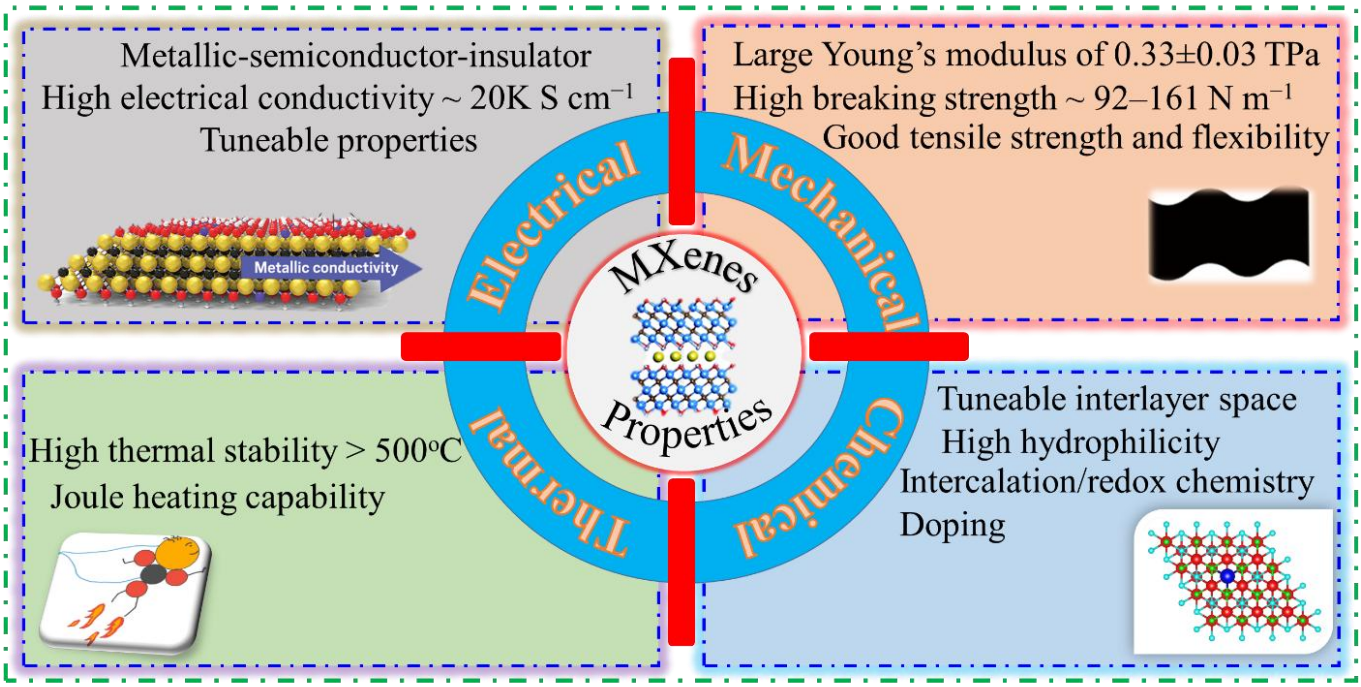

Figure 3. Schematic illustration of the MXenes properties.

MXenes are generally chemically stable in a wide range of electrolytes, enhancing the durability and cycle life of devices; this stability is crucial in extending the lifespan [59]. MXenes can be easily functionalized or modified to improve their electrochemical performance; for example, different surface terminations and intercalations can be applied to tailor their properties to specific device requirements [60]. These unique properties of MXenes make them promising materials for improving the electrochemical performance of energy storage devices. Therefore, using MXenes in various components of devices, energy density, power density, and overall device lifespan can be enhanced, leading to more efficient and longer-lasting energy solutions [61]. Here, in this section, we briefly study the properties of MXenes, such as electrical, mechanical, chemical, and thermal properties.

3.1. Electrical properties of MXenes

The 2D MXenes are well known due to their electrical properties that have been extensively studied using theoretical calculations, and multiple investigations show the enormous range of fascinating electrical properties that may be obtained by varying compositions [62]. Like the MAX phases, the $M_3X_2T_x$, $M_4X_3T_x$, and $M_5X_3T_x$ MXenes are metallic, resulting in strong electric conductivity due to the M-*d* states close to the Fermi level [63]. The electrical conductivity of MXene also depends on surface termination groups: MXene with fluorine surface termination has metal-like conductivity, and MXene with oxygen termination group shows semiconductor-like conductivity [64]. The semiconductor-to-metallic varying electronic properties of MXene are due to M and X elements. Numerous M_2XT_x compounds with surface terminations, including Ti_2CO_2, Sc_2CF_2, and $Sc_2C(OH)_2$, have a semiconducting character, according to first-principles calculations [62]. Similarly, the blade-coating process was used to create $Ti_3C_2T_x$-MXene, which had a strong electrical conductivity of 20 $kScm^{-1}$ [65]. At very low temperatures (less than 10 K), Nb_2CT_x-MXene showed superconductivity with surface functional groups of S, Se, Cl, and NH [66]. Robust electrical conductivity makes fast electron/ion transmission conceivable and avoids needing an individual conductive substance or current collector [67]. The electrical properties of MXene enhance the electrochemical performance in various energy storage and conversion applications.

3.2. Mechanical properties of MXenes

2D MXenes, due to their ability to fold, roll, and twist mechanically, with exceptional mechanical properties because of the strong covalent bond between transition metal elements and carbon and nitrogen, quickly satisfy the needs of energy storage/conversion applications [68]. According to theoretical calculations, pristine MXene, like M_2XT_x with M = Ti, Hf, Mo, Sc, and Zr, has a tensile strength of approximately 92 –161 N m^{-1}, proving it to be intensely mechanically stable [69]. The Young's modulus of the $Ti_3C_2T_x$-MXene monolayer was measured by the elastic modulus tester and atomic force microscopy (0.33 TPa), which is more than 2D materials produced using the solution method [70]. The MXene flakes decorated into thin films using the hydrazine foaming method create porous MXene foams that are freestanding, flexible, hydrophobic in nature, and lightweight [71]. Different surface termination groups also affect MXene mechanical properties; MXene with oxygen ─O surface termination is more elastic, rigid, and stiffer than with surface termination ─F and ─OH [64]. MXenes have several outstanding potentials that make them the perfect candidate to be utilized as a material for an electrode in flexible energy storage and conversion applications, including bending resistance, flexibility, and high tensile strength. The study of the mechanical properties of MXene provides a way to understand the importance of MXene in EES applications and energy conversion devices because of their exceptional physicochemical merits, multilayered structures, flexibility, and excellent strength.

3.3. Chemical properties of MXenes

The early transition metals of MXenes, such as Ti, Nb, and Ta (M-layers), are nonreactive and generate different MXene compositions with variable spacing between layers [72]. The fascinating features of 2D-MXene materials, such as high SSA, high melting point, low toxicity, significant electrical conductivity, and abundant redox surface, were created during the etching of AI layers in the MAX phases [73]. This will

enhance the electrochemical performance of MXene material in energy storage applications and energy conversion devices [73]. The surface functionalized groups provide a highly hydrophilic nature to MXene and make it soluble in water. Heteroatom doping impacts the Fermi level, ion transport, and MXene bandgap. Dopants with specific valance, boding, and dimension configurations will function better for storage/conversion [74]. Due to MXenes' versatility, they can serve various valuable applications, such as energy storage devices, water purification, lubrication, photocatalysis etc. Its exceptional electrical thermoelectric and optical properties make MXene suitable for multiple applications [75]. Most investigations on MXenes also reveal that they have a variety of unique physical and chemical characteristics, including ion mobility, structural characteristics, and electronic transport features, making them attractive with improved electrochemical properties for use in electrochemical energy storage and energy conversion [76].

3.4. Thermal properties of MXenes

The wide range of oxidation properties displayed by dry MXene affects the thermal stability of $Ti_3C_2T_x$-MXenes', and these characteristics are influenced by both the chemical makeup of the material and the presence of an oxidizing environment. At 200 °C and 1000 °C, respectively, $Ti_3C_2T_x$-MXene partly oxidizes to TiO_2 (anatase) in an oxygen environment, while it oxidizes to CO_2 and H_2O at 1000 °C in an air environment [77]. In an argon environment, Ti_2CT_x-MXene survives in temperatures up to 375 °C but in the air only up to 150 °C [78, 79]. In the chemical expression of MXene M_nT_x, the stability of MXene increases by increasing the value of *n,* which decreases MXene; the lesser the binding energy, the more stable MXene will be [80]. The vacuum-assisted filtration process fabricated thin $Ti_3C_2T_x$-MXene film arrays that exhibit exceptional high-temperature thermal camouflage capabilities for indoor and outdoor applications. These $Ti_3C_2T_x$-MXene thin films offer a wide temperature range of thermal camouflage, ranging from -10 °C to over 500 °C. Additionally, they have a significantly lower radiant temperature (higher than 300 °C for an object above 500 °C), long-term stability in high temperatures or flames, strong electromagnetic interference shielding efficiency, and adaptable concealed Joule heating capacity [81]. The characteristics of thermodynamically metastable MXene have exposed metal atoms on the surface, possess high surface energies, and oxidize spontaneously in the air [78]. The thermal conductivity of MXenes can also facilitate heat dissipation, making it more reliable for EES applications and conversion.

4. MXenes for Energy Storage Applications

Electrochemical energy storage (EES) devices, including Sc, SCs, and RBs, are on the front line in addressing the rising need for high-energy devices among the many energy storage technologies [25, 34]. Although there are significant advancements in Sc, SCs, and RBs, utilization of such EES still has some significant obstacles at the grid scale. For instance, attaining elevated power density and energy density simultaneously and the unaffordability of EES devices are substantial obstacles to its wide application use [82, 83]. Recently, MXene, a newly discovered material belonging to the 2D family, is a promising electrode material for electrochemically based Sc, SCs, and RBs [34, 84]. MXenes possess enormous electrical conductance properties, mechanical properties, SSA, and functionalized surfaces of transition metals, making them suitable electrode materials for high energy and power density [36, 37]. The charge storage mechanism in MXene material is based on pseudocapacitive storage, where quick ion intercalation occurs between MXene layers. The MXene layers are stacked to reduce the time active sites are exposed to the electrolyte while allowing quick intercalation, and this combination produces the charge storage density-specific capacitance without sacrificing cycle life or power density [85, 86]. Considering the superior electrochemical properties of pristine MXenes, several difficulties exist, including the layer aggregation and restacking of MXenes caused by hydrogen bonding and vdW interactions [87, 88]. Due to this, the utilization of MXene's effectiveness for high-performance ESDs as an electrode is zhampered. MXene decorated composite with other materials

[89, 90] to stop it from restacking, oxidizing, and degrading is one of the simplest ways to overcome the limits of MXene discussed above.

4.1. MXenes-Based Electrode Materials for Supercapacitors

SCs, due to their substantial cycle life, elevated power density, and quick charging-discharging rate, have shown to be the most advantageous options [91, 92]. SCs can compete with RBs, although their energy density is much lower; this necessitates additional studies to address these issues and investigate useful electrode materials without losing the SCs' power density for next-generation devices [93]. 2D MXenes have demonstrated remarkable electrochemical characteristics due to their strong metallic conductance, transition metal content, and hydrophilicity of their ─OH or ─O terminal groups [63, 94, 95]. Fast ion transit and higher ion accessibility provided by MXenes-based composites improved the performance of SCs [96]. Therefore, ongoing research and development in this area aims to investigate and maximize the potential of MXenes, advancing high-performance and energy-efficient SCs.

111111

Recently, Javed et al. [97] utilized a one-step hydrothermal process for embedding nickel–cobalt–sulfide (NCS) nanoflowers heterostructure (HS) into exfoliated $Ti_3C_2T_x$–MXene layers (HS−NCS@MXene). The NCS nanoflowers were uniformly distributed and formed a sandwich-like shape in layers of MXene. In assembling HS−NCS@MXene//AC–AHSC, the negative electrode was of activated carbon (AC) material, and the positive electrode was of HS−NCS@MXene composite material. The AHSC delivered a specific capacitance of F g^{-1} at 1.5 A g^{-1} with a steady cyclic life of 92% up to 20,000 cycles when operated in a potential range up to 1.6 V. Additionally, AHSC exhibited high power density (1196 W kg^{-1}) and an energy density (80 Wh kg^{-1}); therefore, HS system gave exceptional electrochemical properties for AHSCs due to the combined effectiveness of NCS and MXene. The scanning electron microscopy (SEM) in Fig. 4(a). demonstrated the NCO nanoparticles sulfurization and vulcanization into NCS nanoflowers, which were then more equally distributed on the surface of MXene nanosheets.

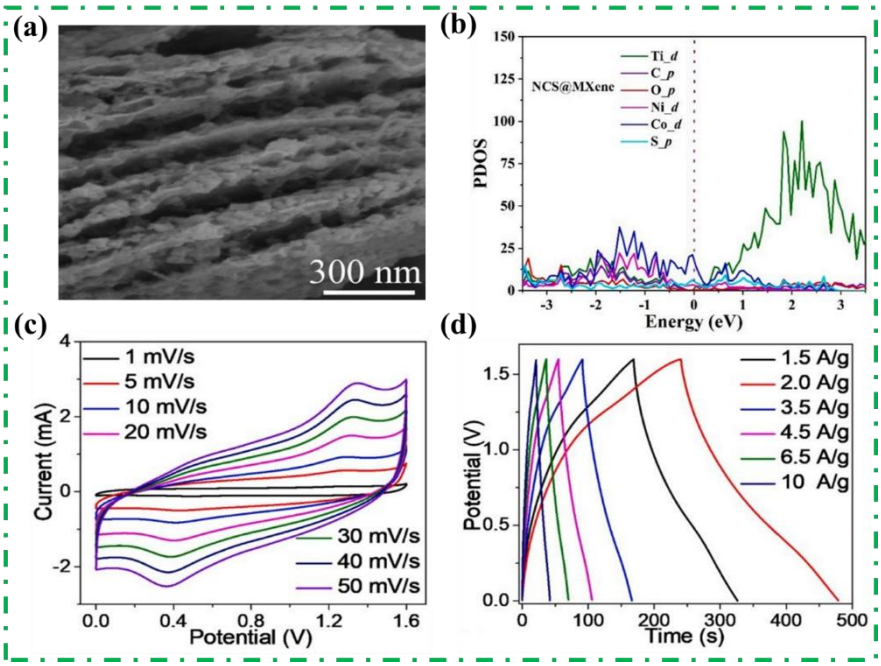

Figure 4. (a) HR-SEM image of HS−NCS@MXene, (b) The PDOSs of the HS−NCS@MXene, (c) CV profile at different scan rates, (d) GCD profile at different current densities, reproduced from ref [97] Copyright (2022), reproduced with permission from Elsevier.

Furthermore, the impact of the HS−NCS@MXene was examined by density functional theory (DFT) simulations. The HS system had improved conductivities with metallic characteristics compared to the NCS and MXene as it crossed the Fermi level with stronger states (Fig. 4(b)). In Fig. 4(c), the cyclic voltammetry (CV) profile of the AHSC are represented at various scan rates from 1 to 50 mVs^{-1} in the voltage range from 0.0 to 1.6 V. All CV profile contained a discernible pair of redox peaks, indicating a hybrid-pseudocapacitive charge storage mechanism. The remarkable reversibility and stability of the AHSC were further ensured by the well-maintained shapes of CV curves at high scanning speeds. Fig. 4(d) shows the GCD profile recorded at different current densities (1.5 to 10 A g^{-1}) in the voltage range of 0.0 to 1.6 V. The virtually symmetrical GCD curves with a little voltage drop showed good electrochemical reversibility and respectable Coulombic efficiency.

4.2. MXenes-Based Electrode Materials Capacitors

Thanks to the high SSA, large interlayer spacing, and outstanding electrical conductivity, MXenes The Li^+, Na^+, K^+, or Zn^+ diffusion processes can quickly transfer electrons [98, 99]. However, the restacking problem of 2D MXene hampers electrode and electrolyte interaction suppresses their capacities and rate capabilities, lowering EES's electrochemical performance [100]. Anodes and cathodes for lithium-ion capacitors (LICs) are based on those used in batteries. Because of their exceptional energy and power density, primarily governed by their anode and cathode's physical and chemical parameters, they can be attractive candidates for future EES systems [101]. Furthermore, sodium-ion capacitors (NICs) have shown their promising use in upcoming low-cost energy storage technologies [102]. The rapid storing characteristic of Na^+-ions in the electrode material determines how quickly these devices can operate. The development of potassium-ion capacitors (KICs), which have an anode as a battery type and a cathode as a capacitor type and exhibit Faradaic and non-Faradaic reaction processes, has been proposed [103, 104]. High power, energy density, and suitable cycle life are all possible with the hybrid mechanism and "accordion-type" reaction process. However, creating appropriate electrode materials is extremely difficult because of the enormous radius of K^+ [105]. Zinc-ion capacitors (ZIHCs) employ anodes of Zn metal and gained popularity because of their low redox potential, environment-friendly nature, and sizeable theoretical capacity [106, 107].

Using a Na-biphenyl radical anion complex solution, Naguib et al. [108] reported Na pre-intercalated MXene with a high concentration (up to 2 Na per $Ti_3C_2T_x$ formula). Combining computational simulations with an investigation of the neutron pair distribution function revealed several sodiation sites and the creation of 2D sodium domain structures at interfaces and surfaces. On a small scale, the density functional tight-binding (DFTB) approach identified the presence of Na^+-ions that greatly impacted the induced layer charges and the oxidation/reduction process. The pre-sodiated MXene's electrochemical performance in Na^+-ion Cs demonstrated outstanding reversibility and promise during testing. To further comprehend element-specific charge shifts in layers of $Ti_3C_2O_2$-MXene, Fig. 5(a) displays a sample snapshot from a DFTB simulation. The Mulliken population analysis described the electronic charge distributions before and after sodiation, and the straight black line showed that each atom had its charges before sodiation. The CV profile at 0.1 mVs^{-1} is demonstrated in Fig. 5(b); as Na was already present between the layers of the sodiated samples' $Ti_3C_2T_x$, the testing of CV began with the charging procedure (from open-circuit voltage to 3.0 V vs. Na/Na^+). A prominent irreversible sodiation peak was visible in pristine $Ti_3C_2T_x$ (without pre-sodiation) at 0.5 V vs. Na/Na^+. The irreversible peak for $Na_2Ti_3C_2T_x$ and $Na_1Ti_3C_2T_x$ was less than that of pristine $Ti_3C_2T_x$, while there was no discernible peak for $Na_{0.5}Ti_3C_2T_x$. As seen in Fig. 5(c), $Na_2Ti_3C_2T_x$, which had more pre-intercalated Na than $Na_1Ti_3C_2T_x$ and $Na_{0.5}Ti_3C_2T_x$, had a higher first-cycle de-sodiation capacity than those two compounds. The charge/discharge profiles for $Na_2Ti_3C_2T_x$, $Na_1Ti_3C_2T_x$, and $Na_{0.5}Ti_3C_2T_x$ are shown in Fig. 5(d) at various testing rates.

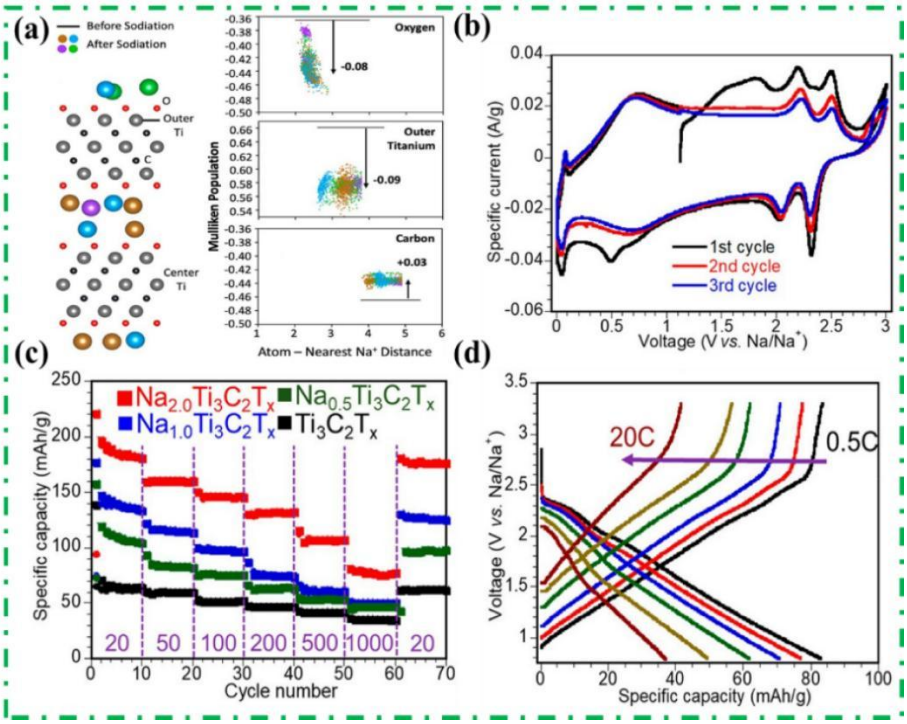

Figure. 5. (a) Sodiated MXene ($Na_1Ti_3C_2O_2$) structure, presenting the four sodiation sites correlation to the $Ti_3C_2O_2$ layers, the corresponding Mulliken charge populations, (b) CV curves, (c) First GCD cycles, (d) Charge−discharge curves, reproduced from ref [108], Copyright (2021), with permission from the American Chemical Society.

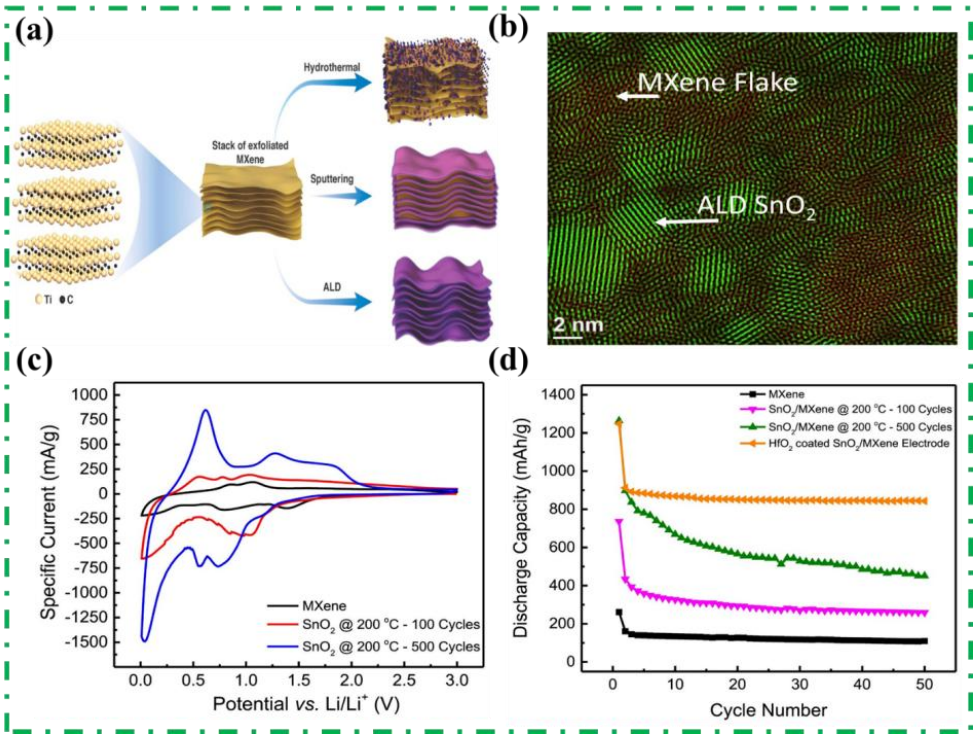

Figure. 6. (a) Schematic representation of methods used for deposition SnO_2 material on Ti_3C_2 MXene nanosheets, (b) a Fourier-filtered HR image, (c) Comparison of the first cycle of CV, (d) Cyclic performance, reproduced from ref [118] Copyright (2017), with permission from Elsevier.

The identical morphologies of all the charging/discharging profiles, including behavior like that of a capacitor or battery, proved that the observed capacity resulted from a mix of structure–controlled processes and sodium ion diffusion.

4.3. MXenes-Based Electrode Materials for Batteries

Lithium-ion batteries (LIBs) offer prominent energy densities for hand-held electric devices and electric cars [83, 109]. The high-performing electric vehicles and energy storage applications at large scale, such as electric plants and grid applications, need high energy and power density; this could prevent LIBs from fully meeting these demands [110]. Contrarily, monovalent non-lithium alkali metals (Na^+, K^+) and multivalent metals (Zn^{2+}, Mg^{2+}, and Al^{3+}) have attracted much interest [111-113]. Therefore, new batteries are being developed as low-cost, high-safety battery alternatives; for instance, Na^+-ion batteries (NIBs), K^+-ion batteries (KIBs), and Zn^{2+}-ion batteries (ZIBs), Mg^{2+}-ion batteries (MIBs) and Al^{3+}-ion batteries (AIBs) [114-117]. Advanced battery electrodes should generally withstand repeated charging/discharging cycles of different RBs while maintaining electron/ion transport and structural durability, which calls for materials for electrodes with appropriate physicochemical features and good electrochemical properties [114, 116]. But as no electrode material on the market today completely satisfies these stringent requirements, effective efforts are underway to research and meticulously build new materials for electrodes methodically. MXenes, however, are intriguing materials for battery applications due to their distinctive characteristics.

Alshareef et al. [118] used atomic layer deposition (ALD) to grow SnO_2/MXene sheets and fabricated a composite anode for LIBs applications. The anode preserved the structural and mechanical reliability of the MXene substrate while taking advantage of the high Li^+-ion capacity provided by SnO_2. The ALD conditions were utilized to coat SnO_2 on MXene, concluded with ─O, ─F, and ─OH groups, and it was discovered that these groups were crucial for halting MXene breakdown. Fig. 6(a) demonstrated a graphical representation of three distinct processes and impacts on MXene sheets by these processes. During hydrothermal synthesis, the high temperature, pressure, and aqueous environment results in the development of SnO_2 particles on deformed MXene nanosheets. A Fourier-filtered HRTEM picture of MXene containing SnO_2 crystallites is displayed in Fig. 6(b) to demonstrate the dispersion of SnO_2 on MXene sheets.

The CV profile of the MXene-electrode and SnO_2/MXene hybrid electrodes are shown in Fig. 6(c) and were calculated at a scan rate of 0.2 mVs^{-1} in the potential range of 0.01 to 3.00 V (vs. Li/Li^+). The cathodic peaks were observed: three were large, and two were small at 1.39, 1.18, 0.78, 0.50, and 0.01 V, respectively, in the first cathodic scan of the as-prepared MXene-electrode. The following cycles saw the disappearance of the prominent peaks at 1.39 and 0.78 V, which was attributed to the Li^+ ions becoming trapped between MXene sheets. The third prominent peak at 0.01 indicates the carbon lithiation in the anode material. The cyclic performance of SnO_2-coated MXene anodes was evaluated in range (100 to 1000 mAg^{-1}); however, Fig. 6(d) compares the results at 500 mAg^{-1}. The as-prepared MXene exhibited a first-cycle discharge capacity of 260 $mAhg^{-1}$; after 50 cycles, it displayed a consistent capacity of 109 $mAhg^{-1}$. The first-cycle discharge capacity of the SnO_2/MXene composite anode was 736 $mAhg^{-1}$, and after 50 cycles, it maintained a steady 258 $mAhg^{-1}$ capacity.

Through experimental and theoretical studies, Yao et al. [119] verified that $MoSe_2$/MXene possessed better electrochemical performances and electronic properties than MoS_2/MXene. The electronic properties calculations revealed that MXenes mainly contributed to the HS system's conductivity; however, $MoSe_2$/MXene showed a slightly lower diffusion barrier than MoSSe/MXene. The conductions of related HS systems, for instance, MoSSe/MXene, were superior to $MoSe_2$/MXene, particularly when the Se was coupled with MXene. The results of the calculations also showed that MoSSe/Ti_3C_2-MXene was more appropriate for NIB anodes since it had a more excellent theoretical value of capacity (593.3 mAh/g) and a lesser open circuit potential of 1.538 V than $MoSe_2$/Ti_3C_2-MXene. Fig. 7(a) displays the XRD patterns of $MoSe_2$/$Ti_3C_2T_x$ composite

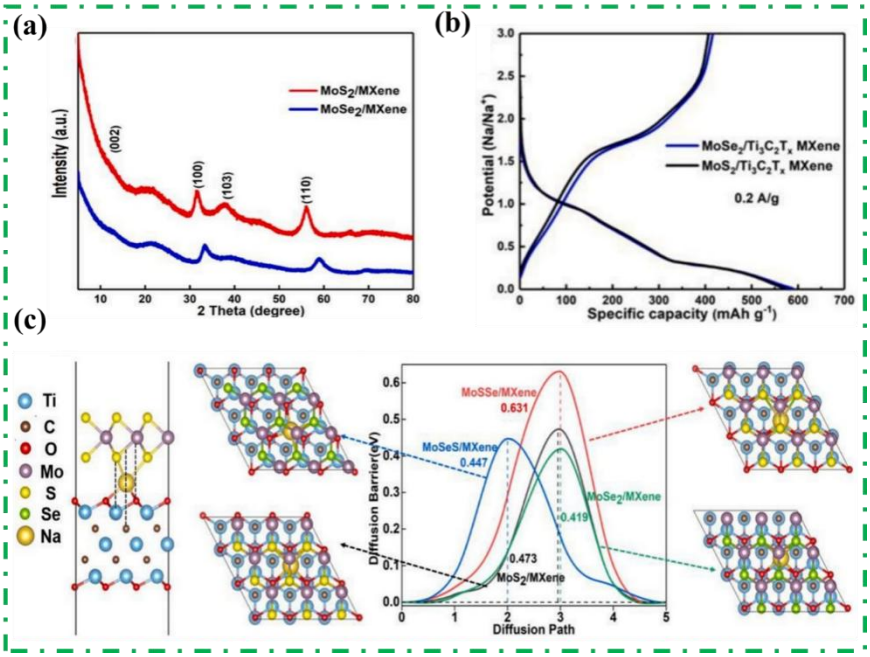

Figure. 7. (a) XRD patterns, (b) Initial discharge/ charge curves, (c) Stable position Na in the interlayer of HS, diffusion barriers of Na, and saddle points, reproduced from ref [119], Copyright (2023), with permission from Elsevier.

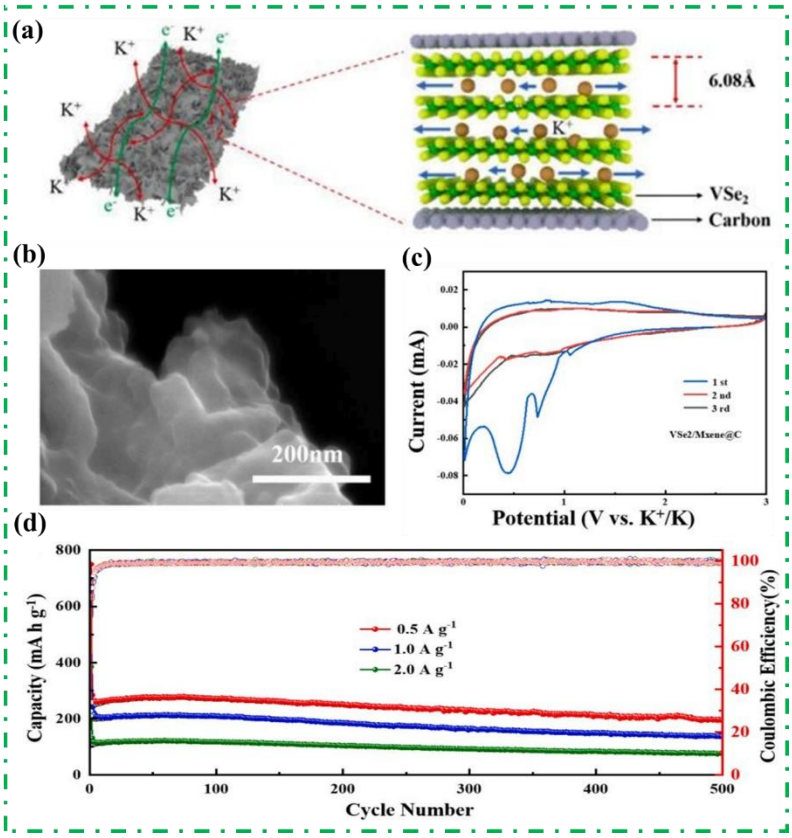

Figure. 8. (a) Schematic illustration of paths for the diffusion of K+, structural model of VSe2/MXene@C, (b) FESEM image, (c) CV curves, (d) Cycling capacity in the long-term, reproduced from ref [120] Copyright (2022), with permission from Elsevier.

and $MoS_2/Ti_3C_2T_x$ HS systems, which showed a small oxidization peak at 25°, caused by CTAB's hydrothermal oxidation protection. $Ti_3C_2T_x$ MXene's surface-grown $MoSe_2$ and MoS_2 efficiently prevented their unfavorable spontaneous accumulation. Fig. 7(b) depicts the GCD profile of both HS systems at 0.2 Ag^{-1}, sloping without a plateau section, and $MoSe_2$/MXene offered a greater initial capacity than MoS_2/MXene. Two HS systems' initial discharge/charge capacities were 571.7/407.3 $mAhg^{-1}$ and 588.4/416.6 $mAhg^{-1}$, respectively, with an initial Coulombic efficiency (ICE) of 70%. Fig. 7(c) depicts the location of Na inserted into HS layers, which was similar to the Na when it was adsorbed on just the two components, and offered the energy barriers of HS systems were 0.473, 0.631, 0.447, and 0.419 eV, respectively. The structure interlayer spacings at the saddle point were also estimated, as seen in Fig. 7(c). A slight energy barrier was offered by shifting the position of the saddle point of the MoSeS/MXene hybrid structure to the left.

Through the hydrothermal method, Liu et al. [120] successfully fabricated the VSe_2/MXene@C with a hierarchical three-dimensional (3D) structure. A VSe_2/MXene@C composite with a hierarchical 3D structure was developed using excellent mechanical strength and superior electrical conductivity of MXene. In particular, strong covalent interactions between VSe_2 nanosheets and O atoms on MXene substrates secured the nanosheets to the surface. Covering the carbon layer also prevented VSe_2/MXene degradation and significantly increased the battery's capacity and cycling stability. The VSe_2/MXene@C demonstrated exceptional electrochemical performance and had the potential to be an ideal candidate for material for the anode in KIBs. The schematic illustration and structural model in Fig. 8(a) show the paths for the diffusion of K^+-ions in the VSe_2/MXene@C. Field-emission scanning electron microscopy (FESEM) examined the morphologies and microstructures of as-prepared materials. The VSe_2/MXene image (Fig. 8(b)) shows that VSe_2 flakes were heaped or embedded vertically on MXene substrates. Further, CV profile curves were examined at 0.01 to 3 V with fresh K foils serving as the reference and counter electrodes. According to Fig. 8(c), the CV profile first cycle at 0.1 mV s^{-1} with a potential of 0.01 to 3V shows prominent cathodic peaks at 0.75 and 0.5V, respectively, but they disappeared in the following cycles, suggesting the occurrence of a solid-electrolyte interphase (SEI) film on VSe_2/MXene@C hybrid surface. According to Fig. 8(d), VSe_2/MXene@C possessed specific capacitance of 197 at 500 mA g^{-1}, 138.7 at 1000 mA g^{-1}, and 77.2 mAh g^{-1} at 2000 mA g^{-1} after 500-cycles. Additionally, the long cycle process had nearly no unusual charging or discharging behaviors, and the Coulombic efficiency remained constant at a high level.

Further, Gao et al. [121] prepared a Ti_3C_2-MXene-based hybrid by growing 1T-MoS_2 *in-situ* on Ti_3C_2 MXene, presented a successful method for creating a 3D-linked charge-discharge network HS with enhanced conductivity and reliable chemical coupling. By inventively fusing metallic 1T-MoS_2 nanosheets with conductor Ti_3C_2 MXene, larger 1T-MoS_2 interlayers were produced from 9.5 to 9.9 Å and improved hydrophilicity. Highly stable cycling over time and remarkable high-rate capabilities were both displayed by novel-prepared HS. The metallic 1T-MoS_2's high capacity was due to the enlarged ion storage space that resulted from the layers' wider spacing. The effective synergistic interaction of both materials in the 3D interconnected networks was ascribed to the notable long-term cycle stability. Under various bending situations, the wearable quasi-solid-state ZIB with the 1T-MoS_2/Ti_3C_2-MXene composite cathode showed steady electrochemical properties. The phase and crystal structures of the samples demonstrated by the XRD patterns in Fig. 9(a); the peaks situated at 2θ of 14.1, 33.2, and 58.8° were determined to correspond to index (002), (100), and (110) peaks of the 2H-MoS_2. However, the peak located at 2θ of 9.3° was classified as the (002) peak of the 1T-MoS_2. Fig. 9(b) depicts the reaction mechanism; as the discharge-charge process progressed, Zn^{2+}-ions were reversibly inserted and extracted at the cathode, along with an oxidation/reduction

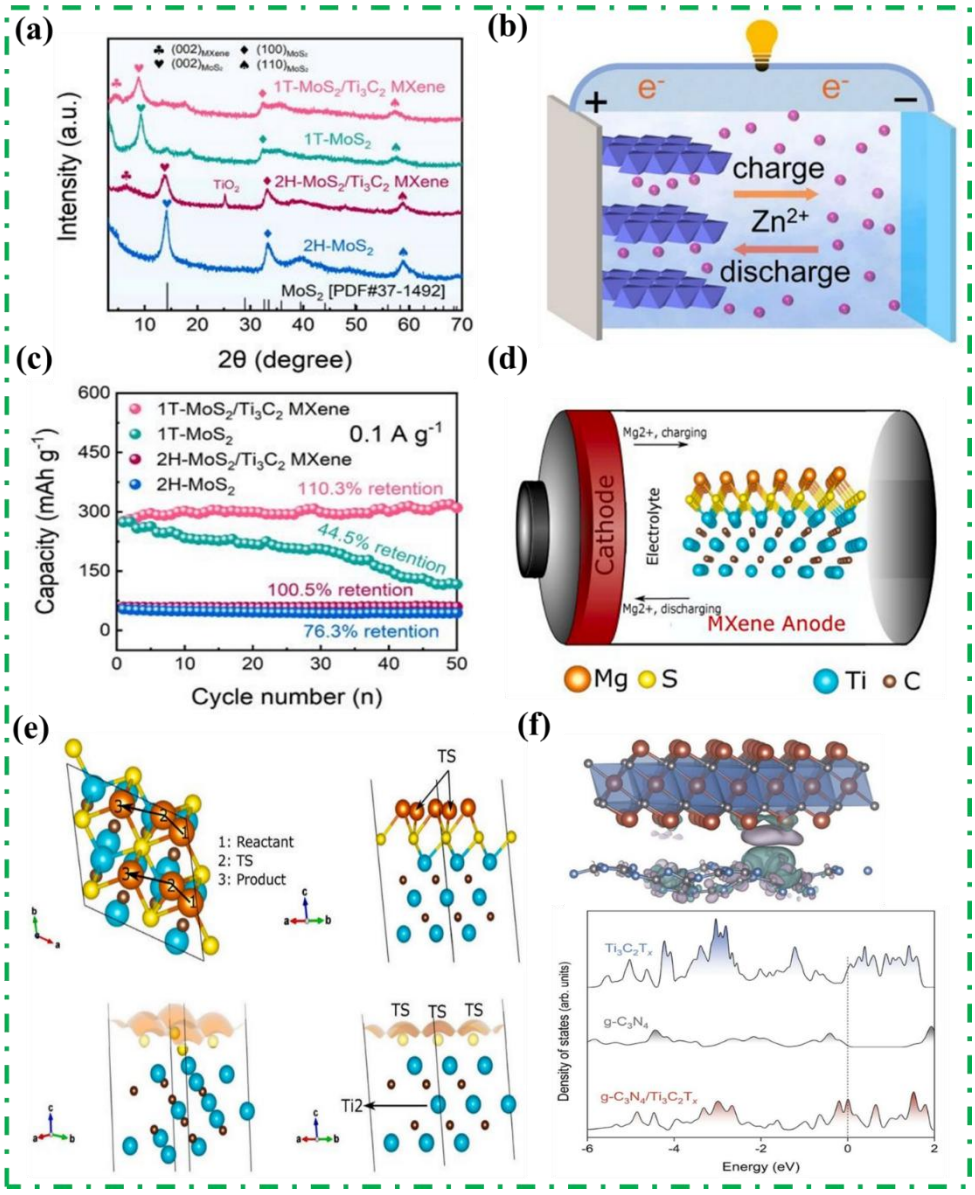

Figure. 9. (a) XRD patterns, (b) Schematic of the mechanism of Zn^{2+}-ion batteries, (c) Cycling performance, reproduced from ref [121], Copyright (2023), with permission from Elsevier. (d) The working mechanism of MIB battery, (e) Supercell of the $Ti_3C_2S_2$–Mg MXene layer along top and front views, showing the reactant, TS, and Mg^{2+}-ion, while arrow shows the direction of the diffusion, reproduced from ref [122] Copyright (2022), with permission from Elsevier. (f) DOS of three materials and CDD of Al^{3+} on g-C_3N_4/$Ti_3C_2T_x$ hybrid, reproduced from ref [123] Copyright (2022), with permission from Elsevier

reaction at the anode. A decent specific capacity (105.2 mAh g^{-1} at 10.00 A g^{-1}) was obtained, maintaining 36.9% of the capacity attained at 0.10 A g^{-1}. The 1T-MoS_2/Ti_3C_2 MXene electrode exhibited excellent cycling stability with 93.2% capacity retention after 3000 cycles at a 1.0 A g^{-1} and 110.3% after 50 cycles (Fig. 9(c)).

Christopoulos et al. [122], for the first time using DFT calculations, reported the $Ti_3C_2S_2$-MXene structure and studied its adsorption and diffusion energies of an Mg^{2+}-ion on the surface of the MXene. They found very strong adsorption and the lowest energy barrier for Mg diffusion in Ti_3C_2-based materials reported so far. Fig. 9(d) shows a detailed schematic illustration of the working cycle of $Ti_3C_2S_2$-MXene anode using Mg^{2+}-ions. The above illustration indicates that using

$Ti_3C_2S_2$ as an anode electrode in MIB potentially ensured faster charge/discharge rates than in the LIB case, as the Mg^{2+}-ions will be much more mobile than the Li^+-ions. During charging, Mg^{2+} ions leave the positive electrode (cathode) and move through the electrolyte to the negative electrode (anode). Fig. 9(e) shows the transition state (TS), and it was found that Mg^{2+}-ion sat at the fcc position, thus following the Ti_2 – fcc – Ti_2 path. The energy barrier for diffusion of the Mg^{2+}-ions on the surface of the $Ti_3C_2S_2$-MXene monolayer was 0.049 eV.

Chen et al. [123] designed a g-C_3N_4/$Ti_3C_2T_x$ HS to address the issue of aluminum-storage capacity and rate, which offers a conductive supporting framework to maintain structural integrity and accelerate electronic transport. The energy storage mechanism of the g-C_3N_4/$Ti_3C_2T_x$ HS cathode was demonstrated as the reversible intercalation of $AlCl_4$–during cycling. The battery-capacitance model mechanism in the g-C_3N_4/$Ti_3C_2T_x$ HS accelerated the kinetics of the electrode reactions. DFT calculations certified that g-C_3N_4/$Ti_3C_2T_x$ HS possesses enhanced electrical conductivity and Al^{3+}-ion trapping capability. As illustrated in the upper panel of Fig. 9(f), the g-C_3N_4/$Ti_3C_2T_x$ hybrid displayed the most robust interaction with Al and the lowest binding energy, corresponding to the excellent ionic trapping capabilities and stability of heterojunction, which was beneficial for Al adsorption. The density of state (DOS, Fig. 9(f) lower panel) revealed that the g-C_3N_4/$Ti_3C_2T_x$ composite afforded the highest DOS value at the Fermi level among three active materials, suggesting that the constructed heterojunction enhanced the electrical conductivity of the electrode material.

5. MXenes for Energy Conversion Applications

Energy conversion research is increasingly being investigated theoretically and empirically; in terms of energy conversion devices, layered MXene material uses are generally well-reported [124-126]. Numerous applications, including catalysis, triboelectric generators, photovoltaic electrodes, and thermoelectric generation, have shown how MXenes can convert energy. MXene, a large family of 2D nanomaterials, is appealing for various applications due to its physicochemical diversity [127]. Recently, the studies revealed the potential of pristine-MXene and MXene-based composite in energy conversion applications. MXenes have a more adaptable composition, structure, and surface chemistry than other 2D materials, and their advantageous features, including metallic conductance, redox activity, hydrophilic nature, and plasmonic behavior, make it a promising material to utilize in various energy conversion applications [128]. The MXene material showed extraordinary electronic properties because of its intrinsic metallic nature and, when used as catalysts, can significantly benefit remarkable electrochemical reactions: oxygen reduction reaction (ORR) is a critical process in fuel cells, oxygen evolution reaction (OER) in the fuel cell, and hydrogen evolution reaction (HER) [129-131]. MXenes are efficient catalysts that increase energy conversion efficiency in fuel cells and electrolyzers because of their strong electrical conductance, tuneable surface chemistry, and substantial surface area. Excellent electrocatalytic activity for water splitting, a necessary step in creating hydrogen as a clean and renewable energy source, has been demonstrated using MXenes. Due to high electrical conductance, large surface area, and sizeable interlayer distance, MXenes are efficient photocatalysts for various reactions, including water splitting and pollutant degradation [130]. The potential of MXenes is still being explored and optimized to advance high-performance and effective energy conversion systems.

5.1. MXenes for Catalysts

The catalysts based on MXene material are frequently used in catalytic reactions like OER ORR [132-134]; the electrocatalytic mechanisms, as well as the design of MXene materials, are still up for debate; even the mechanisms predicted by computational studies are still empirical. To find highly effective and stable MXene-based catalysts, it is essential to identify the catalytic pathways using *in-situ* characterization methods and quantum chemical calculations. A promising HER electrocatalyst is believed to be an MXene with an O terminal because of the mechanism that maximizes activity in combination with it [135].

The catalyst performance dramatically depends upon the

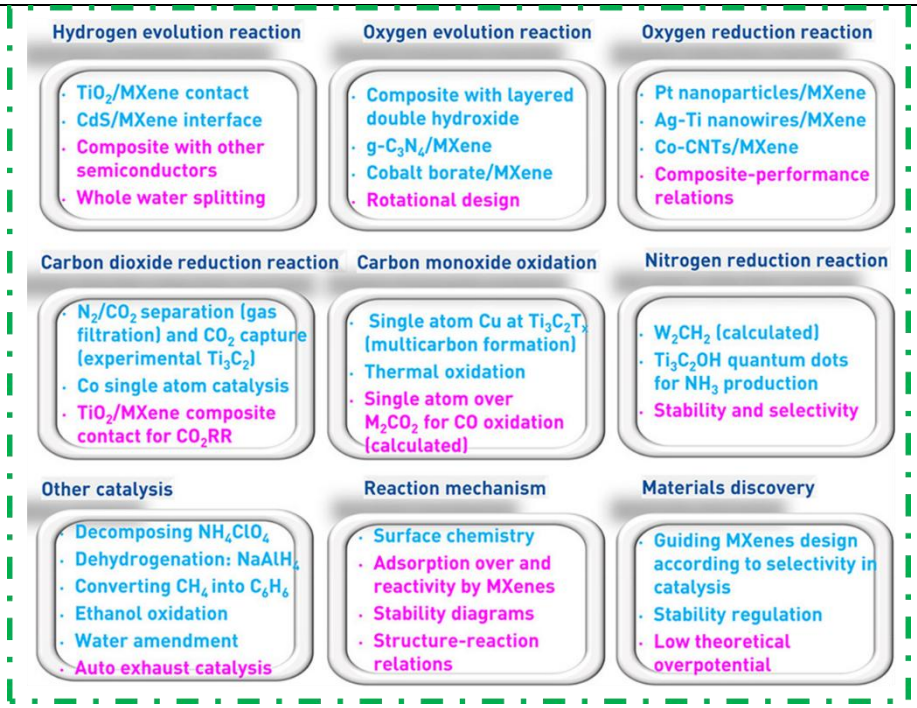

Figure 10. MXene-based catalysis current progress in blue and future trends in purple, reproduced from ref [130], Copyright (2022), with permission from the American Chemical Society.

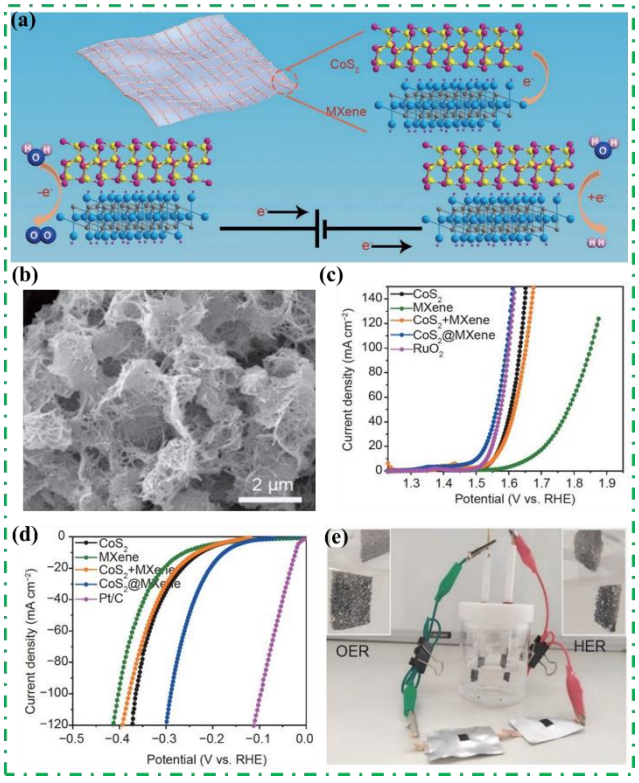

Figure 11. (a) Schematic illustration of the overall water splitting mechanism, (b) SEM image of CoS_2@MXene hybrid, (c-d) The OER and HER polarization curves, (e) Water splitting device, reproduced from ref [143], Copyright (2021), with permission from the Springer Nature.

nature of the MXene functional groups (─O, ─F, and ─OH) [136, 137]. MXene-based composite layered double hydroxides and MXenes with hydroxyl group enriched have been found to have good OER activity owing to their fascinating metallic feature and attractive electronic structure [138]. The booming development of catalysts witnessed some of the catalysts based on MXene material showing comparable or even better performance than benchmark catalysts [139]. Pristine-MXenes have not yet demonstrated sufficient ORR activity, and MXenes containing F groups are potential ORR candidates [140, 141]. However, Pt SACs embedded on MXenes sheets have demonstrated excellent ORR activity performance in DFT computations [142]. Fig. 10 summarizes the development of MXenes in energy conversion (catalysis-based), and the future trends are indicated in each panel's purple-colored bottom rows. MXenes are attractive materials for catalysts for various applications because of their distinctive qualities, including high surface area, tuneable electrical characteristics, stability, and adaptability.

Peng et al. [143] reported an all-in-one electrocatalyst system for ORR, OER, and HER in water splitting by efficient interface engineering between MXene and highly active electrocatalytic species (CoS_2) through an *in-situ* hydrothermal growth and facile sulfurization process. The CoS_2@MXene electrocatalyst comprised one-dimensional (1D) CoS_2 nanowires and 2D MXene nanosheets, which led to a hierarchical structure, spatial electron redistribution, and high anchoring strength. Therefore, the electrocatalyst achieved enhanced catalytic activity and long-time stability for ORR (a half-wave potential of 0.80 V), OER (an overpotential of 270 mV at 10 mA cm^{-2}, i.e., η_{10} = 270 mV) and HER (η_{10} = 175 mV). Fig. 11(a) shows the schematic illustration of the overall water-splitting mechanism of CoS_2@MXene. The SEM (Fig. 11(b)) image's morphologies confirm that the CoS_2 nanowires were parallelly anchored on the isolated MXene nanosheets without apparent aggregation and restacking. Fig. 11(c) shows that among the series of hybrid electrocatalysts with different ratios of CoS_2 to MXene, CoS_2@MXene synthesized with 10 mL of MXene solution exhibited the best OER performance with the lowest overpotential of 270 mV at 10 mA cm^{-2} than CoS_2 (323 mV), MXene (431 mV) and RuO_2 (302 mV). Additionally, CoS_2@MXene also achieved electrocatalytic HER activity in the same measurement condition. The CoS_2@MXene composite displayed a smaller overpotential of 175 mV than CoS_2 (225 mV) and MXene (260 mV) at 10 mA cm^{-2} in Fig. 11(d), which was ascribed to the synergistic effect between CoS_2 and MXene. Based on the electrochemical performance in both OER and HER processes, CoS_2@MXene composites were adopted as bifunctional electrodes to assemble into the water-splitting system, as shown in Fig. 11(e).

5.2. MXenes for Solar Cells

MXenes are suitable materials for solar cell application because of their excellent photoelectrochemical characteristics [144]. Their distinct electronic structure and strong electrical conductivity improve the solar cells' performance. In the visible region and near-infrared portions of the electromagnetic spectrum, MXenes show widespread absorption. They can catch a more significant percentage of solar light thanks to their broad absorption spectrum, which improves solar energy conversion efficiency [145, 146]. Due to their advantageous energy band alignment and charge transport features, MXenes can successfully separate photoexcited electron-hole pairs. The efficiency of solar cells is enhanced by the effective charge separation and transport that prevents recombination and loss of photo-generated charges [147].

Even when exposed to extreme climatic conditions, MXenes display outstanding stability and endurance. This stability is essential for solar cells' long-term performance and dependability, assuring their efficacy over time [148]. Different transition metals can be used to synthesize MXenes, resulting in a range of compositions and characteristics. Due to their adaptability, MXenes can be optimized for various solar cell types, including organic, dye-sensitized, and perovskite solar cells [149]. MXenes are simple to include in current solar cell topologies and production techniques. They are appealing for practical implementation in solar cell devices

because of their compatibility with various substrates and electrode materials. MXenes have much potential for solar cell applications, but more work is needed to improve their characteristics, increase their effectiveness, and investigate new device topologies [150]. Despite this, MXenes are a promising material for enhancing solar cell technology and assisting in creating sustainable energy solutions due to their distinct properties.

Including a 2D-layered $Ti_3C_2T_x$-MXene into the precursor and, for the first time, incorporating it into the perovskite absorber layer, Ma et al. [151] revealed a novel method to change the perovskite layer to increase efficiency. According to the findings, $CH_3NH_3PbI_3$ crystal size increased due to $Ti_3C_2T_x$ termination groups delaying crystallization. It was discovered that MXene's strong electrical conductance and mobility accelerated the transfer of charge. After the critical parameters were optimized, the device's performance was improved by 12% with the help of 0.03 wt% of MXene addition. The nucleation and development path of a perovskite film containing the addition of MXene material is represented in Fig. 12(a).

The performance of the devices is shown in Fig. 12(b) with and without additive modification. The device's photon-to-electron conversion efficiency (PCE) was lower than that of the devices with additions of 0.01, 0.02, and 0.03 wt%. The maximum PCE of 17.41% was obtained for the 0.03 wt% additive–based device in the reverse scan with J_{sc}, V_{oc}, and filling factor (FF) of 22.26 mA cm^{-2}, 1.03 V, and 0.76, respectively, compared to the pristine device's 15.54%, 20.67 mA cm^{-2}, 1.00 V, and 0.75. Further, J_{sc} was improved in a 0.03 0.03 wt% additive–incorporated device, which agreed with the incident PCE. The device conductivity was evaluated using the electrochemical impedance spectrum (EIS) method illustrated in Fig. 12(c).

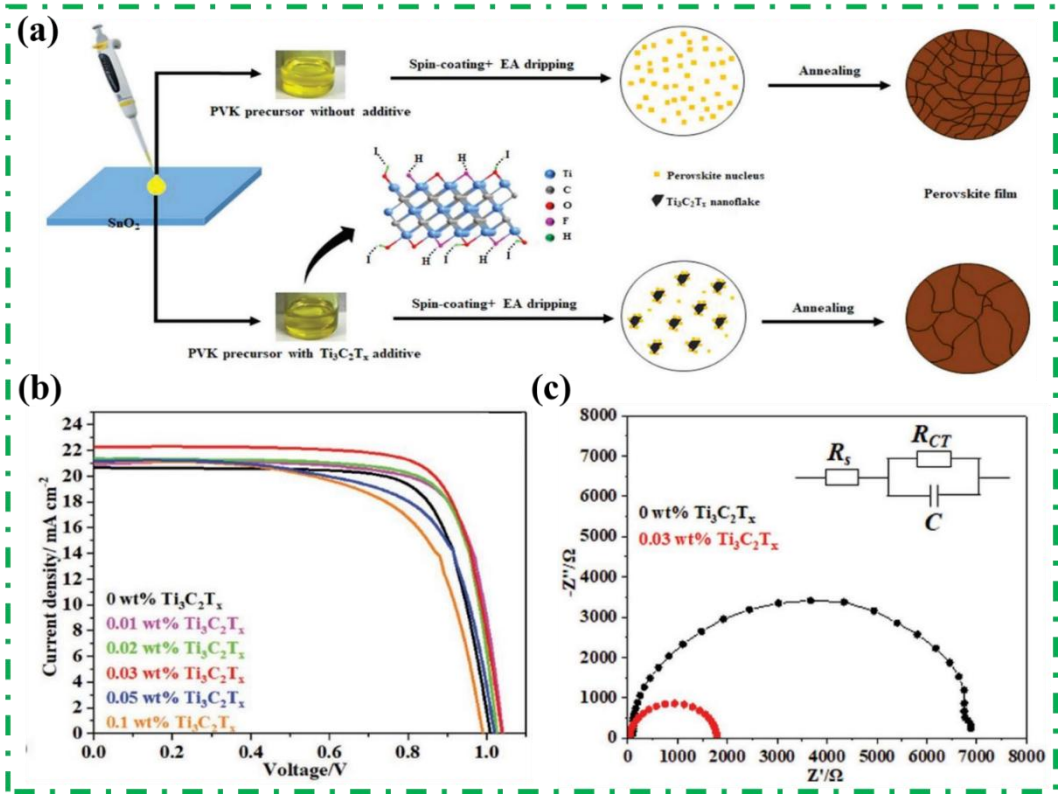

Figure 12. (a) Proposed nucleation and growth route, (b) *J–V* curves, (c) Nyquist plots, reproduced from ref [151], Copyright (2018), with permission from John Wiley and Sons.

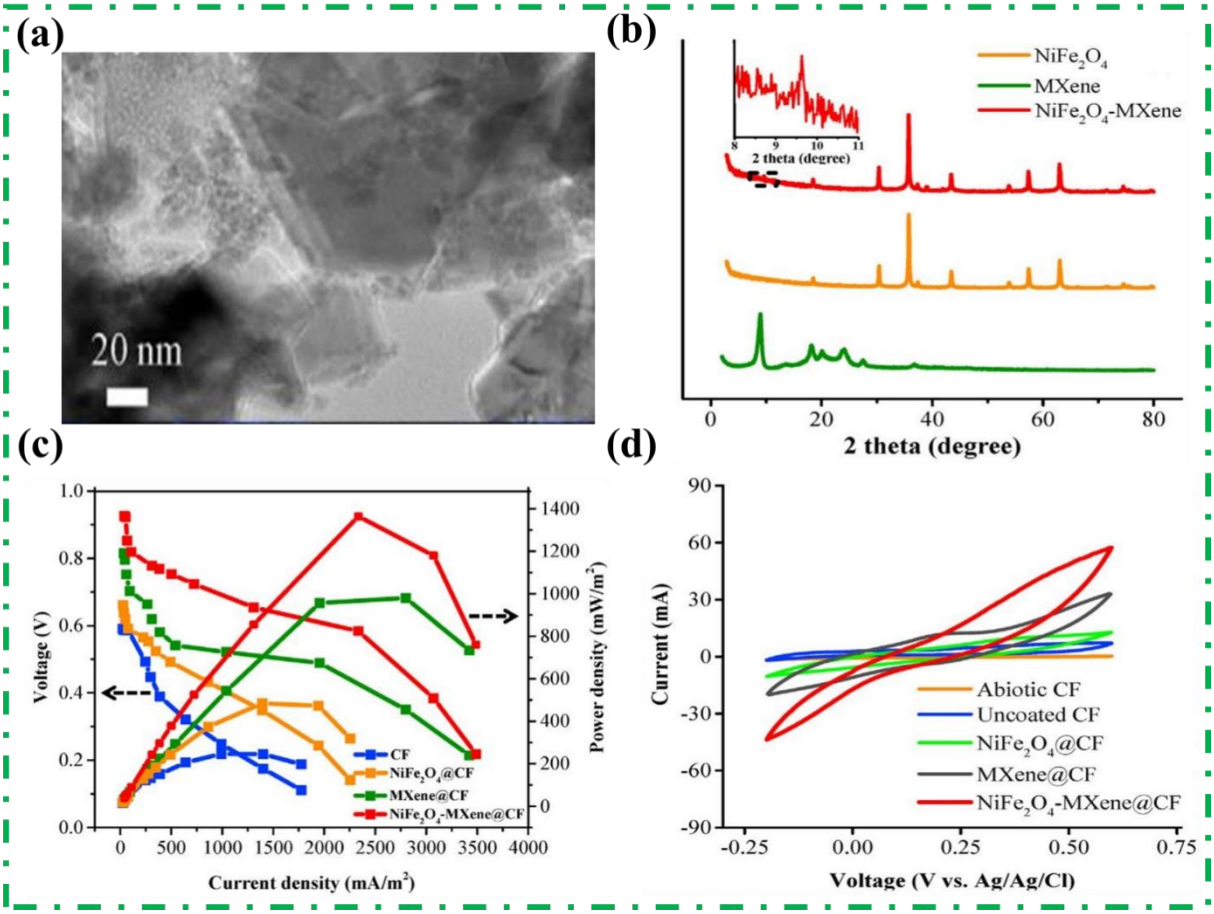

Figure 13. (a) HR-TEM image, (b) XRD pattern, (c) polarization and power density profile, (d) CV profile of biotic and abiotic electrode systems, reproduced from ref [158], Copyright (2021), with permission from Elsevier.

The acquired results demonstrated a decrease in charge transfer resistance (R_{CT}) from 7000 -1800 Ω, indicating conductivity growth of the perovskite coating. As a result, the $Ti_3C_2T_x$ additive's strong electrical conductivity and mobility helped to improve the J_{sc} by lowering charge transfer resistance and promoting charge transfer.

5.3. MXenes for Fuel Cells

Excellent catalytic activity is exhibited by MXenes, especially in the electrochemical reactions in fuel cells [152]. Their large surface area and distinctive electronic structure enable effective catalysis of various processes, including ORR and HER, and their catalytic activity boosts the performance and efficiency of fuel cells [153].

In fuel cells, MXenes can act as a supporting component for other catalysts and improve the stability and toughness of catalyst components, halting degradation and extending their useful life. A conductive channel for electron transfer can also be provided by MXenes, enabling effective charge transport in the fuel cell [154]. MXenes have layered structures with nanoscale channels, allowing effective gas diffusion and transportation inside the fuel cell. This characteristic is essential for feeding reactants to the catalyst sites, such as oxygen and hydrogen, and eliminating reaction byproducts from the fuel cell, such as water vapor. Even in the challenging working environments of fuel cells, MXenes are renowned for their outstanding stability and corrosion resistance [155]. This stability guarantees the fuel cell's long-term performance and durability, lowering the need for routine maintenance and material replacement.

MXenes can be made using several transition metals, allowing

their characteristics to be tailored for specific fuel cell applications [156]. Due to their adaptability, MXenes can be optimized for use in fuel cells: proton exchange membrane fuel cells (PEMFCs) and solid oxide fuel cells (SOFCs), as catalysts, catalytic supports, or gas diffusion layers [155]. MXenes are appealing for large-scale fuel cell production because they can be made using a reasonably easy and scalable procedure [157]. They are a possible replacement for traditional fuel cell materials because of their affordability and appealing qualities. In conclusion, MXenes provide unique benefits for fuel cell applications, including catalytic activity, electrocatalyst support, gas diffusion properties, stability, adaptability, scalability, and affordability.

Using simple dip-and-dry and hydrothermal techniques, Lee et al. [158] utilized $NiFe_2O_4$ ($NiFe_2O_4$@CF), MXene (MXene@CF), and $NiFe_2O_4$-MXene ($NiFe_2O_4$-MXene@CF) to modify a typical carbon felt (CF) electrode. The electrochemical performance of these modified CF electrodes was much enhanced, and $NiFe_2O_4$-MXene@CF obtained the maximum power density of 1385 mW m^{-2}, which was 5.6 times greater than that of CF, 2.8 times greater than that of $NiFe_2O_4$@CF, and 1.4 times greater than that of and MXene@CF anodes, respectively. The HR-TEM image in Fig. 13(a) depicts the fine $NiFe_2O_4$ dispersion over the MXene structure, providing a rougher electrode surface for microbial attachment. A TEM image showed that the composite comprised $NiFe_2O_4$ nanoparticles with Ni, Fe, and O uniformly dispersed on its surface and coupled with MXene nanosheets. Additionally, according to XRD patterns, the characteristic MXene peaks were found at 8.8 and 18.1, which correspond to the (002) basal plane and (004) in-plane diffraction, respectively (Fig. 13(b)). Further, no peak was observed at 39, corresponding to an Al (104) plane and showing that it was removed entirely via HF etching, enabling the effective creation of a 2D structure of MXene. These microbial growth-promoting gap forms in the MXene nanosheets enhanced the production of biofilms and the efficiency of the microbial electrosynthesis system. The spinel cubic structure of $NiFe_2O_4$ showed characteristic peaks at 18.4, 30.2, 35.7, 37.3, 43.3, 53.8, 57.4, 62.9, and 74.5, which corresponded to the (111), (220), (311), (222), (400), (422), (511), (440), and (220) planes, respectively.

The MFC performance of the modified electrodes was assessed using Fig. 13(c), which compares the polarization and power density profile while adjusting the external resistance. All modified electrodes demonstrated enhanced power density compared to the uncoated CF anode. The $NiFe_2O_4$-MXene@CF anode exhibits an elevated power density of 1385 mW m^{-2}, which was 5.6, 2.8, and 1.4 times more than that of the CF, $NiFe_2O_4$@CF, and MXene@CF anodes, respectively. The composite creation of $NiFe_2O_4$ with the MXene nanosheets resulted in a significant increase of anode current, the MXene electrical conductance, and the existence of many redox-active centers in $NiFe_2O_4$ led to better CV outcomes, as indicated in CV analysis (Fig. 13(d)). The substantial rise in electron transfer over the other evaluated electrodes demonstrated $NiFe_2O_4$-MXene@CF's better electrochemical capacity for electrogenesis.

6. Conclusion and Future Outlook

Creating innovative materials for EES and conversion applications greatly aids the progress of a viable environment. 2D MXenes are intriguing materials because they have highly conductive layered structures that can accommodate different ions and tuneable surface chemistry and have the potential to modify surface redox processes. Due to the several advantages, MXenes have gained significant attention, making them suitable for various energy storage and conversion devices. Their excellent electrical conductivity allows them for efficient charge transfer and high-power output. MXenes possess a high surface area, which benefits EES applications and provides more sites for ions to adsorb, leading to higher capacitance and energy storage capacity. The layered structure of MXenes allows for fast ion diffusion, enabling rapid charge and discharge rates, which are crucial for quick energy release. They are chemically stable, even in harsh environments, and their stability is advantageous for long-term use in EES and conversion devices, ensuring durability and reliability. MXenes serve multiple functions in one device, such as

simultaneously acting as an electrode and a catalyst, reducing the need for additional materials and improving device efficiency. MXenes have shown potential for hydrogen storage applications due to their ability to adsorb and release hydrogen efficiently. This review emphasizes MXenes features, briefly explains their crystal structure, and describes their high-performance results in EES and conversion applications. We describe the most recent developments in 2D MXenes for SC, SCs, RBs catalysts, solar cells, and fuel cells. MXene has made considerable strides in recent years, but many obstacles remain to overcome before it can be used in EES and conversion applications.

Authors Contribution

Muhammad Sufyan Javed and Asad Ali Supervision, Conceptualization, Investigation,V alidation, Formalanalysis, Salamat Ali; Writing-originaldraft. Awais Ahmad, Iftikhar Hussain, Syed Shoaib Ahmad Shah and Shafqat Ali: Writing and reviewing manuscript.

Conflicts of Interest

There are no conflicts of interest reported by the writers.

Acknowledgment

This work was financially supported by the Research Fund for International Scientists (52250410342), Scientific Research start-up grant for Youth Researchers at Lanzhou University. Asad Ali thanks the financial support from Kempe Foundation (SMK21-0011, SMK21-0020).

Data Availability statement

The data presented in this study are available on request from the corresponding author.

Funding

Not Applicable (N/A)

REFERENCES

1. Khan, I., et al., Does energy trilemma a driver of economic growth? The roles of energy use, population growth, and financial development. Renewable and Sustainable Energy Reviews, 2021. 146: p. 111157.
2. Joshi, A., et al., Chemical looping-A perspective on the next-gen technology for efficient fossil fuel utilization. Advances in Applied Energy, 2021. 3: p. 100044.
3. Ali, S., et al., 2H-MoS2 nanosheets-based binder-free electrode material for supercapacitor. Journal of Applied Physics, 2022. 132(14): p. 145001.
4. Jun, B.-M., et al., Review of MXenes as new nanomaterials for energy storage/delivery and selected environmental applications. Nano Research, 2019. 12(3): p. 471-487.
5. Sufyan Javed, M., et al., Boosting the energy storage performance of aqueous NH4+ symmetric supercapacitor based on the nanostructured molybdenum disulfide nanosheets. Chemical Engineering Journal, 2023. 471: p. 144486.
6. Zhang, A., et al., MXene-based nanocomposites for energy conversion and storage applications. Chemistry–A European Journal, 2020. 26(29): p. 6342-6359.
7. Zhang, X., et al., Exploring the origin of pseudocapacitive energy storage differences for molybdenum nitride-based electrodes. Chemical Engineering Journal, 2023. 462: p. 142250.
8. Neto, P.B.L., O.R. Saavedra, and D.Q.J.R.E. Oliveira, The effect of complementarity between solar, wind and tidal energy in isolated hybrid microgrids. Renewable Energy, 2020. 147: p. 339-355.
9. Parkash, A., et al., Heteroatom-Doped High Porous Carbon Metal Free Nanomaterials for Energy Storage and Conversion. ECS Journal of Solid State Science Technology, 2022.
10. Evliya, H., Energy Storage for Sustainable Future—A Solution to Global Warming, in Thermal Energy Storage for Sustainable Energy Consumption. 2007, Springer. p. 87-99.
11. Javed, M.S., et al., The quest for negative electrode materials for Supercapacitors: 2D

materials as a promising family. Chemical Engineering Journal, 2023. 452: p. 139455.

12. Li, D., et al., Numerical assessment of a hybrid energy generation process and energy storage system based on alkaline fuel cell, solar energy and Stirling engine. Journal of Energy Storage, 2021. 39: p. 102631.
13. Abualigah, L., et al., Wind, Solar, and Photovoltaic Renewable Energy Systems with and without Energy Storage Optimization: A Survey of Advanced Machine Learning and Deep Learning Techniques. Energies, 2022. 15(2): p. 578.
14. Jeżowski, P., et al., Safe and recyclable lithium-ion capacitors using sacrificial organic lithium salt. Nature Materials, 2018. 17(2): p. 167-173.
15. Javed, M.S., et al., The Emergence of 2D MXenes Based Zn-Ion Batteries: Recent Development and Prospects. Small, 2022. 18(26): p. 2201989.
16. Abdel-Monem, M., et al. Lithium-ion batteries: Comprehensive technical analysis of second-life batteries for smart grid applications. in 2017 19th European Conference on Power Electronics and Applications (EPE'17 ECCE Europe). 2017. IEEE.
17. Mateen, A., et al., Metal-organic framework-derived walnut-like hierarchical Co-O-nanosheets as an advanced binder-free electrode material for flexible supercapacitor. Journal of Energy Storage, 2022. 49: p. 104150.
18. Choudhary, N., et al., Asymmetric supercapacitor electrodes and devices. Advanced Materials, 2017. 29(21): p. 1605336.
19. Ding, J., et al., Review of hybrid ion capacitors: from aqueous to lithium to sodium. Chemical reviews, 2018. 118(14): p. 6457-6498 %@ 0009-2665.
20. Jagadale, A., et al., Lithium ion capacitors (LICs): Development of the materials. Energy Storage Materials, 2019. 19: p. 314-329.
21. Mateen, A., et al., Silicon intercalation on MXene nanosheets towards new insights into a superior electrode material for high-performance Zn-ion supercapacitor. Journal of Energy Storage, 2023. 71: p. 108151.
22. Javed, M.S., et al., High performance solid state flexible supercapacitor based on molybdenum sulfide hierarchical nanospheres. Journal of Power Sources, 2015. 285: p. 63-69.
23. Li, W., et al., Electric-Field-Triggered Graphene Production: From Fundamental Energy Applications to Perspectives. Accounts of Materials Research, 2022.
24. Fan, F.R., et al., Emerging beyond-graphene elemental 2D materials for energy and catalysis applications. Chemical Society Reviews, 2021. 50(19): p. 10983-11031.
25. Naguib, M., et al., Two-dimensional nanocrystals produced by exfoliation of Ti3AlC2. Advanced materials, 2011. 23(37): p. 4248-4253.
26. Anasori, B., M.R. Lukatskaya, and Y.J. Gogotsi, 2D metal carbides and nitrides (MXenes) for energy storage. Nature Reviews Materials, 2017. 2(2): p. 1-17.
27. Ali, S., et al., The emergence of density functional theory for supercapacitors: Recent progress and advances. Journal of Energy Storage, 2023. 73: p. 109100.
28. Levitt, A., et al., MXene-based fibers, yarns, and fabrics for wearable energy storage devices. Advanced Functional Materials, 2020. 30(47): p. 2000739.
29. Chhattal, M., et al., Unveiling the tribological potential of MXenes-current understanding and future perspectives. Advances in Colloid Interface Science, 2023: p. 103021.
30. Liu, A., et al., Recent progress in MXene-based materials: potential high-performance

electrocatalysts. Advanced Functional Materials, 2020. 30(38): p. 2003437.

31. Zang, X., et al., Enhancing capacitance performance of Ti3C2Tx MXene as electrode materials of supercapacitor: from controlled preparation to composite structure construction. Nano-Micro Letters, 2020. 12(1): p. 1-24.
32. Hui, X., et al., Low-temperature reduction strategy synthesized Si/Ti3C2 MXene composite anodes for high-performance Li-ion batteries. Advanced Energy Materials, 2019. 9(33): p. 1901065.
33. Gogotsi, Y. and P.J.s. Simon, True performance metrics in electrochemical energy storage. science, 2011. 334(6058): p. 917-918.
34. Anasori, B., M.R. Lukatskaya, and Y. Gogotsi, 2D metal carbides and nitrides (MXenes) for energy storage. Nature Reviews Materials, 2017. 2(2): p. 1-17.
35. Barsoum, M.W., The MN+ 1AXN phases: A new class of solids: Thermodynamically stable nanolaminates. Progress in solid state chemistry, 2000. 28(1-4): p. 201-281.
36. Pang, J., et al., Applications of 2D MXenes in energy conversion and storage systems. Chemical Society Reviews, 2019. 48(1): p. 72-133.
37. Yan, J., et al., Flexible MXene/graphene films for ultrafast supercapacitors with outstanding volumetric capacitance. Advanced Functional Materials, 2017. 27(30): p. 1701264.
38. Ando, Y., et al., Capacitive versus pseudocapacitive storage in MXene. Advanced Functional Materials, 2020. 30(47): p. 2000820.
39. Xu, J., et al., Low-Temperature pseudocapacitive energy storage in Ti3C2Tx MXene. Energy Storage Materials, 2020. 33: p. 382-389.
40. Zhang, S. and W.-Q.J.P.C.C.P. Han, Recent advances in MXenes and their composites in lithium/sodium batteries from the viewpoints of components and interlayer engineering. Physical Chemistry Chemical Physics, 2020. 22(29): p. 16482-16526.
41. Thangavel, R., et al., Emerging Materials for Sodium-Ion Hybrid Capacitors: A Brief Review. ACS Applied Energy Materials, 2021. 4(12): p. 13376-13394.
42. Naguib, M., et al., Two-dimensional transition metal carbides. ACS nano, 2012. 6(2): p. 1322-1331 %@ 1936-0851.
43. Kumar, J.A., et al., Methods of synthesis, characteristics, and environmental applications of MXene: A comprehensive review. Chemosphere, 2022. 286: p. 131607.
44. Lei, J.-C., X. Zhang, and Z. Zhou, Recent advances in MXene: Preparation, properties, and applications. Frontiers of Physics, 2015. 10: p. 276-286.
45. Jiang, Q., et al., Review of MXene electrochemical microsupercapacitors. Energy Storage Materials, 2020. 27: p. 78-95.
46. Zhan, X., et al., MXene and MXene-based composites: synthesis, properties and environment-related applications. Nanoscale Horizons, 2020. 5(2): p. 235-258.
47. Naguib, M., et al., Two-Dimensional Nanocrystals Produced by Exfoliation of Ti3AlC2. 2011. 23(37): p. 4248-4253.
48. Sang, X., et al., Atomic Defects in Monolayer Titanium Carbide (Ti3C2Tx) MXene. ACS Nano, 2016. 10(10): p. 9193-9200.
49. Kajiyama, S., et al., Enhanced Li-Ion Accessibility in MXene Titanium Carbide by Steric Chloride Termination. 2017. 7(9): p. 1601873.
50. Feng, A., et al., Two-dimensional MXene Ti3C2 produced by exfoliation of Ti3AlC2. Materials & Design, 2017. 114: p. 161-166.

51. Xie, X., et al., Surface Al leached Ti3AlC2 as a substitute for carbon for use as a catalyst support in a harsh corrosive electrochemical system. Nanoscale, 2014. 6(19): p. 11035-11040.
52. Yang, S., et al., Fluoride-Free Synthesis of Two-Dimensional Titanium Carbide (MXene) Using A Binary Aqueous System. 2018. 57(47): p. 15491-15495.
53. Li, M., et al., Element Replacement Approach by Reaction with Lewis Acidic Molten Salts to Synthesize Nanolaminated MAX Phases and MXenes. Journal of the American Chemical Society, 2019. 141(11): p. 4730-4737.
54. Mei, J., et al., Two-dimensional fluorine-free mesoporous Mo2C MXene via UV-induced selective etching of Mo2Ga2C for energy storage. Sustainable Materials and Technologies, 2020. 25: p. e00156.
55. Zhong, Q., Y. Li, and G. Zhang, Two-dimensional MXene-based and MXene-derived photocatalysts: Recent developments and perspectives. Chemical Engineering Journal, 2021. 409: p. 128099.
56. Al-Hamadani, Y.A., et al., Applications of MXene-based membranes in water purification: A review. Chemosphere, 2020. 254: p. 126821.
57. Li, X., et al., Applications of MXene (Ti3C2Tx) in photocatalysis: A review. Materials Advances, 2021. 2(5): p. 1570-1594.
58. Nan, J., et al., Nanoengineering of 2D MXene-based materials for energy storage applications. Small, 2021. 17(9): p. 1902085.
59. Murali, G., et al., A review on MXene synthesis, stability, and photocatalytic applications. ACS nano, 2022. 16(9): p. 13370-13429.
60. Garg, R., A. Agarwal, and M. Agarwal, A review on MXene for energy storage application: effect of interlayer distance. Materials Research Express, 2020. 7(2): p. 022001.
61. Hui, X., et al., Interface chemistry on MXene-based materials for enhanced energy storage and conversion performance. Advanced Functional Materials, 2020. 30(50): p. 2005190.
62. Khazaei, M., et al., Novel electronic and magnetic properties of two-dimensional transition metal carbides and nitrides. 2013. 23(17): p. 2185-2192.
63. Naguib, M., et al., 25th anniversary article: MXenes: a new family of two-dimensional materials. Advanced materials, 2014. 26(7): p. 992-1005.
64. Bao, Z., et al., Role of MXene surface terminations in electrochemical energy storage: A review. Chinese Chemical Letters, 2021. 32(9): p. 2648-2658.
65. Zeraati, A.S., et al., Improved synthesis of Ti 3 C 2 T x MXenes resulting in exceptional electrical conductivity, high synthesis yield, and enhanced capacitance. Nanoscale, 2021. 13(6): p. 3572-3580.
66. Kamysbayev, V., et al., Covalent surface modifications and superconductivity of two-dimensional metal carbide MXenes. Science, 2020. 369(6506): p. 979-983.
67. Ghidiu, M., et al., Conductive two-dimensional titanium carbide ‘clay’with high volumetric capacitance. 2014. 516(7529): p. 78-81.
68. Ling, Z., et al., Flexible and conductive MXene films and nanocomposites with high capacitance. roceedings of the National Academy of Sciences, 2014. 111(47): p. 16676-16681.
69. Khazaei, M., et al., Electronic properties and applications of MXenes: a theoretical review. Journal of Materials Chemistry C, 2017. 5(10): p. 2488-2503.
70. Lipatov, A., et al., Elastic properties of 2D Ti3C2T x MXene monolayers and bilayers. Science advances, 2018. 4(6): p. eaat0491.

71. Liu, J., et al., Hydrophobic, flexible, and lightweight MXene foams for high-performance electromagnetic-interference shielding. Advanced Materials, 2017. 29(38): p. 1702367.

72. Ghidiu, M., et al., Conductive two-dimensional titanium carbide 'clay' with high volumetric capacitance. Nature, 2014. 516(7529): p. 78-81.

73. Li, X., et al., MXene chemistry, electrochemistry and energy storage applications. Nature Reviews Chemistry, 2022. 6(6): p. 389-404.

74. Kajiyama, S., et al., Sodium-Ion Intercalation Mechanism in MXene Nanosheets. ACS Nano, 2016. 10(3): p. 3334-3341.

75. Ding, L., et al., MXene molecular sieving membranes for highly efficient gas separation. Nature Communications, 2018. 9(1): p. 155.

76. Yu, H., et al., Surface modified MXene-based nanocomposites for electrochemical energy conversion and storage. Small, 2019. 15(25): p. 1901503.

77. Li, Z., et al., Synthesis and thermal stability of two-dimensional carbide MXene Ti3C2. Materials Science and Engineering: B, 2015. 191: p. 33-40.

78. Thakur, R., et al., Insights into the thermal and chemical stability of multilayered V 2 CT x MXene. Nanoscale, 2019. 11(22): p. 10716-10726.

79. Mashtalir, O., et al., Intercalation and delamination of layered carbides and carbonitrides. Nature Communications, 2013. 4(1): p. 1716.

80. Aslfattahi, N., et al., Experimental investigation of energy storage properties and thermal conductivity of a novel organic phase change material/MXene as A new class of nanocomposites. Journal of Energy Storage, 2020. 27: p. 101115.

81. Li, L., et al., Ultrathin Titanium Carbide (MXene) Films for High-Temperature Thermal Camouflage. Advanced Functional Materials, 2021. 31(35): p. 2101381.

82. VahidMohammadi, A., et al., Thick and freestanding MXene/PANI pseudocapacitive electrodes with ultrahigh specific capacitance. Journal of Materials Chemistry A, 2018. 6(44): p. 22123-22133.

83. Ali, S., et al., Recent Advances of Transition Metal Dichalcogenides-Based Materials for Energy Storage Devices, in View of Monovalent to Divalent Ions. The Chemical Record, 2023. n/a(n/a): p. e202300145.

84. Halim, J., et al., X-ray photoelectron spectroscopy of select multi-layered transition metal carbides (MXenes). Applied Surface Science, 2016. 362: p. 406-417.

85. Zheng, S., et al., Ionic liquid pre-intercalated MXene films for ionogel-based flexible micro-supercapacitors with high volumetric energy density. Journal of Materials Chemistry A, 2019. 7(16): p. 9478-9485.

86. Cao, B., et al., Flexible MXene Framework as a Fast Electron/Potassium-Ion Dual-Function Conductor Boosting Stable Potassium Storage in Graphite Electrodes. Advanced Functional Materials, 2021. 31(32): p. 2102126.

87. Wu, Z., et al., The Assembly of MXenes from 2D to 3D. Advanced Science, 2020. 7(7): p. 1903077.

88. Hemanth, N., et al., Transition metal dichalcogenide-decorated MXenes: promising hybrid electrodes for energy storage and conversion applications. Materials Chemistry Frontiers, 2021. 5(8): p. 3298-3321.

89. Zhao, M.Q., et al., Flexible MXene/carbon nanotube composite paper with high volumetric capacitance. Advanced materials, 2015. 27(2): p. 339-345.

90. Li, H., et al., Laser crystallized sandwich-like MXene/Fe3O4/MXene thin film electrodes for flexible supercapacitors. 2021. 497: p. 229882.

91. Wang, W., et al., Hydrous ruthenium oxide nanoparticles anchored to graphene and carbon nanotube hybrid foam for supercapacitors. Scientific reports, 2014. 4(1): p. 1-9.
92. Gui, Q., et al., Scalable Wire-Type Asymmetric Pseudocapacitor Achieving High Volumetric Energy/Power Densities and Ultralong Cycling Stability of 100 000 Times. Advanced Science, 2019. 6(10): p. 1802067.
93. Zhang, X., et al., Chromium induced nickel oxides leads to extraordinary enhancement in the performance of aqueous hybrid supercapacitors. Electrochimica Acta, 2023: p. 143093.
94. Shinde, P.A., et al., Two-dimensional MXenes for electrochemical energy storage applications. Journal of Materials Chemistry A, 2022. 10(3): p. 1105-1149.
95. Kim, H., Z. Wang, and H.N.J.N.E. Alshareef, MXetronics: Electronic and photonic applications of MXenes. Nano Energy, 2019. 60: p. 179-197.
96. Shi, T.-Z., et al., Sea urchin-shaped Fe2O3 coupled with 2D MXene nanosheets as negative electrode for high-performance asymmetric supercapacitors. Electrochimica Acta, 2021. 381: p. 138245.
97. Javed, M.S., et al., Heterostructured bimetallic–sulfide@ layered Ti3C2Tx–MXene as a synergistic electrode to realize high-energy-density aqueous hybrid-supercapacitor. Nano Energy, 2022. 101: p. 107624.
98. Dong, L., et al., Multivalent metal ion hybrid capacitors: a review with a focus on zinc-ion hybrid capacitors. ournal of Materials Chemistry A, 2019. 7(23): p. 13810-13832.
99. Xu, J., et al., An Olefin-Linked Covalent Organic Framework as a Flexible Thin-Film Electrode for a High-Performance Micro-Supercapacitor. 2019. 131(35): p. 12193-12197.
100. Luo, J., et al., Tunable pseudocapacitance storage of MXene by cation pillaring for high performance sodium-ion capacitors. Journal of Materials Chemistry A, 2018. 6(17): p. 7794-7806.
101. Yang, B., et al., Realizing high-performance lithium ion hybrid capacitor with a 3D MXene-carbon nanotube composite anode. Chemical Engineering Journal, 2022. 429: p. 132392.
102. Javed, M.S., et al., Recent progress in the design of advanced MXene/metal oxides-hybrid materials for energy storage devices. Energy Storage Materials, 2022.
103. Hu, X., et al., Fast redox kinetics in bi-heteroatom doped 3D porous carbon nanosheets for high-performance hybrid potassium-ion battery capacitors. Advanced Energy Materials, 2019. 9(42): p. 1901533.
104. Zhang, Z., et al., Fast potassium storage in hierarchical Ca0. 5Ti2 (PO4) 3@ C microspheres enabling high-performance potassium-ion capacitors. Advanced Functional Materials, 2018. 28(36): p. 1802684.
105. Liang, G., et al., Building durable aqueous K-ion capacitors based on MXene family. Nano Research Energy, 2022. 1(1): p. e9120002.
106. Kundu, D., et al., A high-capacity and long-life aqueous rechargeable zinc battery using a metal oxide intercalation cathode. Nature Energy, 2016. 1(10): p. 16119.
107. Zhang, N., et al., Rechargeable aqueous zinc-manganese dioxide batteries with high energy and power densities. Nature communications, 2017. 8(1): p. 405.
108. Brady, A., et al., Pre-Sodiated Ti3C2T x MXene Structure and Behavior as Electrode for Sodium-Ion Capacitors. ACS nano, 2021. 15(2): p. 2994-3003.

109. Choi, C., et al., Achieving high energy density and high power density with pseudocapacitive materials. Nature Reviews Materials, 2020. 5(1): p. 5-19.

110. Zhang, X., et al., Unraveling the improved lithium-storage mechanism by interfacial engineering based on metallic MoS2/MoN heterostructure. Journal of Alloys and Compounds, 2023: p. 171282.

111. Wang, Y., et al., Emerging non-lithium ion batteries. Energy Storage Materials, 2016. 4: p. 103-129.

112. Wang, R., et al., Precise identification of active sites of a high bifunctional performance 3D Co/N-C catalyst in zinc-air batteries. Chemical Engineering Journal, 2022. 433: p. 134500.

113. Zhang, Y.S., et al., Adjustable MXene-Based Materials in Metal-Ion Batteries: Progress, Prospects, and Challenges. SMALL STRUCTURES, 2023.

114. Wu, Y. and Y. Yu, 2D material as anode for sodium ion batteries: Recent progress and perspectives. Energy Storage Materials, 2019. 16: p. 323-343.

115. Song, M., et al., Recent advances in Zn-ion batteries. Advanced Functional Materials, 2018. 28(41): p. 1802564.

116. Kim, H., et al., Recent progress and perspective in electrode materials for K-ion batteries. Advanced Energy Materials, 2018. 8(9): p. 1702384.

117. Aslam, M.K., Y.B. Niu, and M.W. Xu, MXenes for Non-Lithium-Ion (Na, K, Ca, Mg, and Al) Batteries and Supercapacitors. ADVANCED ENERGY MATERIALS, 2021. 11(2).

118. Ahmed, B., et al., Atomic layer deposition of SnO2 on MXene for Li-ion battery anodes. Nano Energy, 2017. 34: p. 249-256.

119. Zhang, W.S., et al., Are Janus MoSSe/Ti3C2-MXene heterostructures excellent anode materials for Na-ion batteries? A computational insight combined experiment. APPLIED SURFACE SCIENCE, 2023. 614.

120. Zhang, H.W., et al., VSe2/MXene composite with hierarchical three-dimensional structure encapsulated in dopamine as an anode for potassium-ion batteries. ELECTROCHIMICA ACTA, 2022. 421.

121. Long, F., et al., Ultrastable and ultrafast 3D charge-discharge network of robust chemically coupled 1 T-MoS2/Ti3C2 MXene heterostructure for aqueous Zn-ion batteries. CHEMICAL ENGINEERING JOURNAL, 2023. 455.

122. Papadopoulou, K.A., A. Chroneos, and S.-R.G. Christopoulos, Mg-ion diffusion on the surface of Ti3C2S2 MXene. Journal of Physics Chemistry of Solids, 2022. 166: p. 110713.

123. Du, Y., et al., Heterostructures assembled from graphitic carbon nitride and Ti3C2Tx MXene as high-capacity cathode for aluminum batteries. Journal of Alloys and Compounds, 2022. 896: p. 162901.

124. Sun, S., et al., Two-dimensional MXenes for energy storage. Chemical Engineering Journal, 2018. 338: p. 27-45.

125. Wei, X., et al., Elucidating the mechanistic origins of P dopants triggered active sites and direct Z-scheme charge transfer by P-MoS2@WO3 heterostructures for efficient photocatalytic hydrogen evolution. Journal of Alloys and Compounds, 2021. 872: p. 159637.

126. Li, J., et al., Ru modulates the catalytic activity of Pt to modify WO3 nanowires for high-performance hydrogen sensing at near room temperature. Applied Surface Science, 2023. 615: p. 156286.

127. Gogotsi, Y. and B. Anasori, The Rise of MXenes. ACS Nano, 2019. 13(8): p. 8491-8494.

128. Gogotsi, Y. and P.J.s. Simon, True performance metrics in electrochemical energy storage. science, 2011. 334(6058): p. 917-918.

129. Wei, X., et al., Carbon intercalated MoS2 cocatalyst on g-C3N4 photo-absorber for enhanced photocatalytic H2 evolution under the simulated solar light. International Journal of Hydrogen Energy, 2023. 48(37): p. 13827-13842.

130. Pang, J., et al., Potential of MXene-based heterostructures for energy conversion and storage. ACS Energy Letters, 2021. 7(1): p. 78-96.

131. Parkash, A., et al., Nickel-Iron-Zinc Phosphide with Three-Dimensional Petal-Like Nanostructure as a Highly Efficient Electrocatalyst for Oxygen Evolution Reaction in Alkaline Electrolytes. ECS Journal of Solid State Science Technology, 2022. 11(8): p. 081008.

132. Wang, H. and J.-M. Lee, Recent advances in structural engineering of MXene electrocatalysts. Journal of Materials Chemistry A, 2020. 8(21): p. 10604-10624.

133. Morales-Garcia, A., F. Calle-Vallejo, and F. Illas, MXenes: new horizons in catalysis. ACS Catalysis, 2020. 10(22): p. 13487-13503.

134. Parkash, A., et al., Highly dispersed Cu nanoparticles decorated on MOF-5: Development of highly efficient noble metal-free electrocatalyst. Nano Futures, 2021. 5(2): p. 025006.

135. Gao, G., A.P. O'Mullane, and A. Du, 2D MXenes: a new family of promising catalysts for the hydrogen evolution reaction. ACS Catalysis, 2017. 7(1): p. 494-500.

136. Chen, Y., et al., V2C MXene synergistically coupling FeNi LDH nanosheets for boosting oxygen evolution reaction. Applied Catalysis B: Environmental, 2021. 297: p. 120474.

137. Chen, J., et al., Vertically-interlaced NiFeP/MXene electrocatalyst with tunable electronic structure for high-efficiency oxygen evolution reaction. Science Bulletin, 2021. 66(11): p. 1063-1072.

138. Ostadhossein, A., et al., Functionalization of 2D materials for enhancing OER/ORR catalytic activity in Li–oxygen batteries. Communications Chemistry, 2019. 2(1): p. 95.

139. Du, C.F., et al., V4c3t x mxene: A promising active substrate for reactive surface modification and the enhanced electrocatalytic oxygen evolution activity. InfoMat, 2020. 2(5): p. 950-959.

140. Kuznetsov, D.A., et al., Single-Atom-Substituted Mo_2 CT_x: Fe-Layered Carbide for Selective Oxygen Reduction to Hydrogen Peroxide: Tracking the Evolution of the MXene Phase. Journal of the American Chemical Society, 2021.

141. Li, Z., et al., The marriage of the FeN4 moiety and MXene boosts oxygen reduction catalysis: Fe 3d electron delocalization matters. Advanced materials, 2018. 30(43): p. 1803220.

142. Liu, C.-Y. and E.Y. Li, Termination effects of Pt/v-Ti n+ 1C n T2 MXene surfaces for oxygen reduction reaction catalysis. ACS Applied Materials Interfaces, 2018. 11(1): p. 1638-1644.

143. Han, S.L., et al., Multi-dimensional hierarchical CoS2@MXene as trifunctional electrocatalysts for zinc-air batteries and overall water splitting. SCIENCE CHINA-MATERIALS, 2021. 64(5): p. 1127-1138.

144. Yin, L., et al., MXenes for Solar Cells. Nano-Micro Letters, 2021. 13(1): p. 78.

145. Fu, H.C., et al., MXene-contacted silicon solar cells with 11.5% efficiency. Advanced Energy Materials, 2019. 9(22): p. 1900180.

146. Ali, S., et al., Layered–Control Approach to Tune The Mobility of Perovskite SrTiO3: A Density

Functional Theory Prospects. ECS Journal of Solid State Science and Technology, 2023. 12(5): p. 054001.

147. Shi, Z., et al., MXene-based materials for solar cell applications. Nanomaterials, 2021. 11(12): p. 3170.

148. Guo, Z., et al., High electrical conductivity 2D MXene serves as additive of perovskite for efficient solar cells. Small, 2018. 14(47): p. 1802738.

149. Li, Z., et al., Single-layered MXene nanosheets doping TiO2 for efficient and stable double perovskite solar cells. Journal of the American Chemical Society, 2021. 143(6): p. 2593-2600.

150. Qamar, S., et al., Recent progress in use of MXene in perovskite solar cells: for interfacial modification, work-function tuning and additive engineering. Nanoscale, 2022. 14(36): p. 13018-13039.

151. Guo, Z.L., et al., High Electrical Conductivity 2D MXene Serves as Additive of Perovskite for Efficient Solar Cells. SMALL, 2018. 14(47).

152. Ahmad Junaidi, N.H., et al., A comprehensive review of MXenes as catalyst supports for the oxygen reduction reaction in fuel cells. International Journal of Energy Research, 2021. 45(11): p. 15760-15782.

153. Fei, M., et al., Polybenzimidazole/Mxene composite membranes for intermediate temperature polymer electrolyte membrane fuel cells. Nanotechnology, 2017. 29(3): p. 035403.

154. Zhao, S., et al., Self-assembly-cooperating in situ construction of MXene–CeO2 as hybrid membrane coating for durable and high-performance proton exchange membrane fuel cell. ACS Sustainable Chemistry, 2022. 10(13): p. 4269-4278.

155. Fan, C., et al., Applications of Two Dimensional Material-MXene for Proton Exchange Membrane Fuel Cells (PEMFCs) and Water Electrolysis. Current Nanoscience, 2021. 17(1): p. 2-13.

156. Hu, X., et al., Synergic degradation Chloramphenicol in photo-electrocatalytic microbial fuel cell over Ni/MXene photocathode. Journal of Colloid Interface Science, 2022. 628: p. 327-337.

157. Jiang, D., et al., Polyaniline-MXene-coated carbon cloth as an anode for microbial fuel cells. Journal of Solid State Electrochemistry, 2022. 26(11): p. 2435-2443.

158. Tahir, K., et al., Nickel ferrite/MXene-coated carbon felt anodes for enhanced microbial fuel cell performance. CHEMOSPHERE, 2021. 268.

How to cite this article:

Ali S,Ahmad A, Hussain I, Shoaib S, Shah A, Ali S, Ali A, Javed MS, (2023). Experimental and Theoretical Aspects of MXenes-Based Energy Storage and Energy Conversion Devices Journal of Chemistry and Environment. 2(2).p. 55-81